Technische Universität München
Fakultät für Physik

Abschlussarbeit im Masterstudiengang Kern-, Teilchen-, und Astrophysik

eV-scale Sterile Neutrino Investigation with the First Tritium KATRIN Data

eV-sterile Neutrino Suche mit den Ersten Tritium Daten von KATRIN

Fotios Megas

29. März 2019

Max-Planck-Institut für Physik

Erstgutachter (Themensteller): Prof. Dr. Susanne Mertens

Declaration of Authorship

English:
I hereby declare that I have written the present Master's thesis in the course Nuclear, Particle and Astrophysics independently, and only with the use of the cited external resources.

Deutsch:
Ich erkläre hiermit, dass ich die vorliegende Abschlussarbeit im Masterstudiengang Kern-, Teilchen-, und Astrophysik selbstständig und nur mithilfe den zitierten Quellen angefertigt habe.

Fotios Megas
Munich, 29.3.2019

Contents

Abstract

Anomalies observed in reactor and accelerator neutrino oscillation experiments may be resolved by the existence of light sterile neutrinos. These hypothetical particles with a mass scale in the range of eV mix with the active neutrinos, distorting their usual oscillation pattern. The KATRIN experiment aims to determine the effective electron antineutrino mass, with an unprecedented sensitivity of 0.2 eV/c^2. Being sensitive to these small neutrino masses, KATRIN can possibly also resolve the anomalies in the oscillation sector. The two main topics of this thesis are 1) the search for light sterile neutrinos in the very first tritium data of the KATRIN experiment and 2) the investigation of the impact of an elevated background on the KATRIN sensitivity to light sterile neutrinos.

Anomalien in Neutrino Oszillations Experimenten sind mit der Einführung von leichten, hypothetischen Teilchen, die sterilen Neutrinos, zu erklären. Diese Teilchen können das gewöhnliche Oszillationsverhalten von Neutrinos verzerren, indem sie dabei auch teilnehmen. Das KATRIN Experiment ist geplant die Neutrinomasse mit einer Sensitivität von 0.2 eV/c^2 zu bestimmen. KATRIN kann also parallel zu der Neutrinomasse Messungen auch möglicherweise diese Anomalien lösen. Die zwei Hauptthemen dieser Arbeit sind 1) die Suche nach sterilen Neutrinos in den ersten Tritium Daten von KATRIN und 2) die Untersuchung der Auswirkung von einer höheren Untergrundsrate auf der Sensitivität von KATRIN bezüglich sterilen Neutrinos.

Chapter 1

Neutrino Physics

1.1 Neutrino History

The neutrino is the lightest fermion and the only particle in the Standard Model of particle physics (SM) that interacts only via the weak interaction. Its elusive nature even nowadays troubles physicists as it still, some 90 years after its postulation by W.Pauli, has some unknown properties.

1.1.1 Postulation and First Detection

In 1930, Pauli proposed in a letter the existence of an electromagnetically neutral particle, which he called the "neutron" [1]. This particle had properties of both the neutron and neutrino, but when J.Chadwick discovered the neutron in 1932 and Fermi published his results on beta-decay, the difference between the two neutral particles was made clear. Without the existence of the neutrino, the nuclear beta-decay would just include the nucleus and the emitted electron, making it a two-body problem. This means that the spectrum would effectively be just a sharp line situated above the maximum (endpoint) energy the electron can get from the decay. The observed spectrum was however a continuous one, which indicated a three-body problem, or in other words, the existence of another particle. This particle would have to be neutral and small compared to the nucleus or else it would have been detected. Thus, the term "neutrino" was coined. It would be 24 years later at the Savanah reactor river site, that the neutrino (actually electron-antineutrino) was detected by F.Reines and C.Cowan [2].

1.1.2 Neutrinos in the Standard Model

In the years that followed, the neutrino was found to have different flavours (electron, muon and tau) and was finally added in the SM as a half-integer, neutral, weakly interacting particle. It was established that the helicity of the neutrino was always negative [3], implying not only that the neutrino has left-handed helicity, but also that it is massless. In the case of massless particles, helicity takes the same

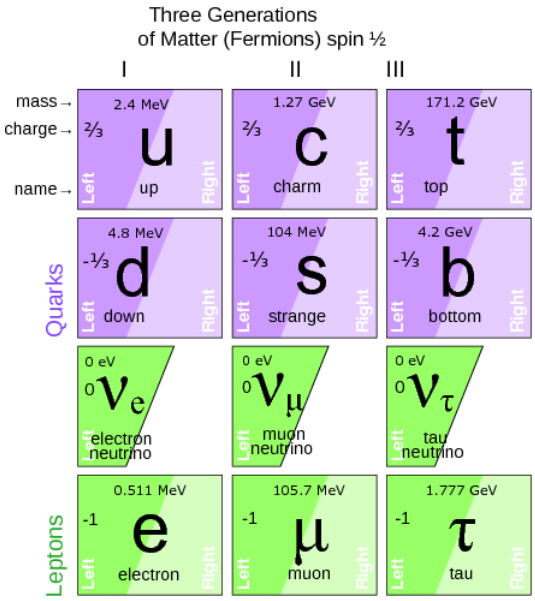

Figure 1.1: The fermion sector of the SM. Neutrinos are the only fields with only one (left) chirality state. Picture taken from [4].

meaning as chirality, meaning that in the case of neutrinos (antineutrinos) right-chiral (left-chiral) fields are absent. The current knowledge of the fermion sector in the SM is shown in figure 1.1.

1.1.3 Neutrino Oscillations

The SM could predict the interactions of neutrinos with great precision until the observation of the so-called neutrino oscillations, where a neutrino produced as a flavor state α has a probability of being detected at a later time at a state β. For this oscillation to take place, the neutrino has to be produced as a definite flavor state and propagate as a mass eigenstate. If neutrinos possess at their birth all three mass eigenstates (which roughly correspond to their three flavors), then these states propagate at different speeds [1], effectively changing the probability of which flavor state the neutrino will later interact as.

The mixing of flavor and mass is dictated by the Pontecorvo-Maki-Nakagawa-Sakata (PMNS) matrix, which is a unitary matrix, almost analog to the CKM-matrix of quark mixing [5]. The mixing then takes the form,

[1] The correct way to phrase this would be that their phases evolve differently with time.

$$\begin{pmatrix} \nu_e \\ \nu_\mu \\ \nu_\tau \end{pmatrix} = \begin{pmatrix} U_{e1} & U_{e2} & U_{e3} \\ U_{\mu 1} & U_{\mu 2} & U_{\mu 3} \\ U_{\tau 1} & U_{\tau 2} & U_{\tau 3} \end{pmatrix} \begin{pmatrix} \nu_1 \\ \nu_2 \\ \nu_3 \end{pmatrix}, \tag{1.1}$$

where $\nu_{e,\mu,\tau}$ are the flavour eigenstates of the neutrino, $\nu_{1,2,3}$ the mass eigenstates and U the PMNS matrix elements. U can be parametrized to depend on three mixing angles and one phase factor. In case of a Majorana neutrino, two more complex phases are added. Although we will work with an antineutrino, the PMNS parametrization holds, with minor sign changes [6].

For a simplified case of two neutrino families, the oscillation probability is given by,

$$P\left(\nu_e \rightarrow \nu_\mu\right) = \sin^2(2\theta)\sin^2\left(1.27\Delta m^2 \frac{L(km)}{E(GeV)}\right), \tag{1.2}$$

with θ the mixing angle, Δm the difference of the mass eigenstates, L the distance to the source, and E the neutrino energy. Neutrino oscillations helped explain the solar neutrino problem, where the neutrino flux detected coming from the sun was not the same as the one predicted by the SM.

Nowadays, neutrino oscillations is a well established fact, proven by a number of experiments [7–10]. This means that neutrinos have a mass in contradiction to the Standard Model, because a zero mass entails a zero oscillation probability. There are many theorized mechanisms to generate a mass for the neutrinos, but here we will show only the most prominent, which focuses on the existence of a so-called "sterile" neutrino.

1.2 Sterile Neutrinos

The most intuitive way to include a neutrino mass in the SM is to include additional neutrino singlet fields with right-handed chirality, ν_R. Then, a mass for the neutrinos can be generated through the Higgs mechanism. This right-handed neutrino would only interact gravitationally, as the weak interaction only couples to left-handed fields. Thus right-handed neutrinos are commonly refered to as "sterile".

The only way for this neutrino to take part in any SM process is through mixing with the active neutrinos. In this case, the PMNS matrix can be extended to a 4x4 matrix [2],

[2] In theory the number of the additional degrees of freedom is not constrained and we could have a (3+N)x(3+N) matrix. Here we just consider the minimal case of one sterile neutrino.

$$\begin{pmatrix} \nu_e \\ \nu_\mu \\ \nu_\tau \\ \nu_s \end{pmatrix} = \begin{pmatrix} U_{e1} & U_{e2} & U_{e3} & U_{e4} \\ U_{\mu 1} & U_{\mu 2} & U_{\mu 3} & U_{\mu 4} \\ U_{\tau 1} & U_{\tau 2} & U_{\tau 3} & U_{\tau 4} \\ U_{s1} & U_{s2} & U_{s3} & U_{s4} \end{pmatrix} \begin{pmatrix} \nu_1 \\ \nu_2 \\ \nu_3 \\ \nu_4 \end{pmatrix}, \tag{1.3}$$

where ν_s is the "flavor" eigenstate corresponding to the right-chiral SM singlet ν_R, and ν_4 the corresponding mass eigenstate.

1.2.1 Theoretical Aspects of Sterile Neutrinos

With the addition of a right-handed neutrino field, neutrinos, as the other fermions, could get their mass with the Higgs mechanism. The most general renormalizable mass terms are

$$\mathcal{L}_{\text{mass}} = -Y^{\nu}_{ij} \bar{L}^i \tilde{H} \nu^j_R - iM_{ij} \left(\nu^i_R\right)^c \nu^j_R + h.c., \tag{1.4}$$

in matrix notation. Here, $\mathcal{L}$ denotes the Lagrangian, Y the Yukawa couplings, L^i the lepton doublet $(\nu_{iL}\ i_L)^T$, with i running through the lepton flavours e, μ, τ, H the Higgs doublet, M_{ij} a Majorana mass matrix, and *h.c.* the hermitian conjugate of the expression. A Majorana mass term implies that neutrinos do not have any quantum numbers at all (and neutrinos would be their own antiparticle, hence lepton number would be violated). We make a distinction by refering to masses arising from the Higgs term as Dirac masses.

After spontaneous symmetry breaking, the Higgs gets a vacuum expectation value and the Dirac mass term can be written as

$$\mathcal{L}_{\text{Dirac}} = \frac{v}{\sqrt{2}} Y^{\nu}_{ij} \bar{\nu}_{iL} \nu^j_R, \tag{1.5}$$

where v is the Higgs vacuum expectation value. Through a basis and slight notation transformation, the mass terms for one generation can take a simple form,

$$\mathcal{L}_{\nu,\text{mass}} = -m\bar{\psi}_L \psi_R - \frac{M}{2} \bar{\psi}_R \psi_R, \tag{1.6}$$

with m being now the Dirac mass, and ψ a spinor containing the ν_L,ν_R fields. Then, the physical masses $m_{1,2}$ are a linear combination of m and M. For a more thorough explanation, the reader is advised to look into [11].

Here, we see that if neutrinos were Dirac particles, M would vanish, leaving one degenerate physical mass $m_{1,2} = m$. For equation 1.3 to hold however, and

sterile neutrino mass eigenstates to be distinguishable from the active neutrino mass eigenstates, neutrinos have to have both Dirac and Majorana masses [3].

This thesis will focus in the case where the Majorana part shares the same scale as the Dirac part. In this case, the mixing between the two is maximal, and additional mass eigenstates can extend the PMNS matrix and allow for neutrino oscillations from and to the sterile state.

1.2.2 Experimental Aspects of Sterile Neutrinos

As stated above, if neutrinos have both Dirac and Majorana masses, active neutrinos would be able to mix with the steriles. Due to their mass scale being quasi-free, sterile neutrinos offer a rich phenomenology. Very heavy ($\sim 10^{18}$ GeV) sterile neutrinos could help solve the matter-antimatter asymmetry in the early Universe through a mechanism called leptogenesis. keV-scale sterile neutrinos could explain a big portion of the Dark Matter. Finally, eV-scale sterile neutrinos could produce visible differences in the oscillation patterns of neutrinos. We opt to focus in the latter, as light sterile neutrinos have the relevant mass scale to produce visible effects in KATRIN.

1.2.2.1 Short Baseline Oscillation Anomaly

The first hint of the existence of a sterile neutrino came from the Liquid Scintillation Neutrino Detector (LSND) experiment [10]. In this experiment, protons with an energy of ~800 MeV were shot at a carbon target, producing pions, which in turn decayed to muons and neutrinos. The LSND experiment is classified as an *appearance* experiment, because it is searching for an excess of $\bar{\nu}_e$ events, oscillating from $\bar{\nu}_\mu$. The beam was directed at liquid scintillation tank, where the neutrinos would interact via leptonic and semi-leptonic processes and inverse β-decay. The accelerated particles were then detected from the Cherenkov radiation they produced.

The results from LSND helped confirm the fact that neutrinos oscillate. However its findings indicated a mass difference of 0.2-10 eV^2 in contradiction to the now well known differences of $\Delta m^2_{12} = 10^{-3}$ eV^2 and $|\Delta m^2_{13}| = 10^{-5}$ eV^2 [12]. This mass difference hinted at the existence of a heavier mass eigenstate, which could be associated with a sterile neutrino in the eV range.

This result was challenged by other similar experiments, being in part confirmed by MiniBoone [13], but also disproven by KARMEN and MINOS [14, 15]. This controversy is still an open issue, as MINOS and MINOS+ were *disappearance* experi-

[3] In the general topic of neutrino oscillations, the term "sterile neutrino" can also be given to particles that mix with the active neutrinos, but are not necessarily right-handed neutrinos. In that case, there are other mass generation mechanisms that will not be discussed in this thesis.

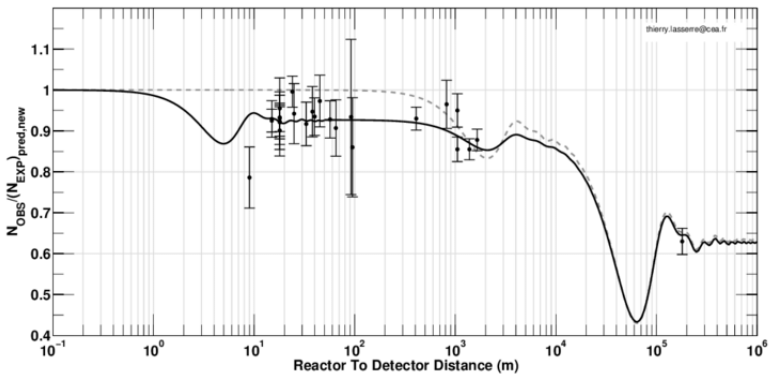

Figure 1.2: Illustration of the short baseline reactor antineutrino anomaly. The observed spectrum is compared to the one predicted without oscillations. The dashed line corresponds to the standard 3 neutrino mixing scheme. The solid line corresponds to an oscillation model including a sterile neutrino. Taken from [20].

ments, meaning they were looking for the absence of neutrino events, making the experiment conceptually different. The tension in appearance and dissapearance data is supposed to reach an ultimatum with the DUNE experiment [16, 17].

1.2.2.2 The Reactor Antineutrino Anomaly

After an update in the lifetime of the neutron and in the antineutrino spectra of different uranium and plutonium isotopes in 2012 [18], neutrino oscillation experiments based on reactors noticed a 6% lower antineutrino event count rate than expected [19]. The remarkable thing was, that this new observation matched the pattern of a light sterile neutrino mixing with the active ones, disfavouring the no-oscillation hypothesis at a 99.8% Confidence Level (C.L.), when combined with other experiments. This was called the Reactor Antineutrino Anomaly (RAA), and was confirmed by almost all reactor experiments. An illustration of the RAA is shown in figure 1.2, where the measured-to-predicted ratio of the antineutrino rate of several experiments is pictured.

Although some reactor experiments are now starting to doubt their physics models [21], the search for light sterile neutrinos is still ongoing in many of them. Recently, the NEOS, DANSS and Neutrino-4 experiments published results in their preliminary analysis, further constraining the sterile neutrino parameter space. Nevertheless, no discovery is claimed in those publications [22–24]. The current

90% C.L. constraints for the sterile neutrino parameters range around 0.2-2.3 eV^2 for the mass difference squared, $\Delta m^2 = m^2_{sterile} - m^2_{active}$, ($m^2_{active} \approx 0$), and below 0.1 for $\sin^2 2\theta$.

The reactor anomaly is to be resolved with current reactor experiments, such as PROSPECT [25] and STEREO [26], which already constrain a relevant part of the parameter space.

1.2.2.3 The Gallium Anomaly

The GALLEX and SAGE experiments were to designed to measure the solar neutrino flux via the reaction $^{71}\text{Ga} + \nu_e \rightarrow {}^{71}\text{Ge} + e^-$. To check the results of these experiments, they were exposed to radioactive ^{51}Cr and ^{37}Ar sources. Both ^{51}Cr and ^{37}Ar decay via e^--capture producing an electron neutrino. The neutrinos are then captured with the same process as for the solar neutrinos.

Both experiments deviated from the expected measured-to-predicted ratio of ^{71}Ge production rate [27]. This anomaly can also be explained by the existence of sterile neutrinos in the eV-scale [28]. Although in the recent years the prefered oscillation parameters from gallium data are in slight tension with the reactor data [29, 30], the anomaly is still not resolved and remains a motivation for the light sterile neutrinos.

1.2.3 Sterile Neutrinos in Cosmology

In cosmology, light sterile neutrinos act as additional relativistic degrees of freedom during primordial nucleosynthesis, impacting several observational parameters.

The effective number of relativistic degrees of freedom N_{eff} can more specifically alter the ^{4}He abundance after nucleosynthesis by making the weak interaction decouple at a larger neutron-to-proton ratio. A major role of N_{eff} is also clear in the Cosmic Microwave Background (CMB), as its behavior can change the expansion rate of the Universe during recombination [31]. In the standard cosmological model without sterile neutrinos, $N_{eff} = 3.046$.

In addition to N_{eff}, a light sterile neutrino would add to the total mass of neutrino species. Low-mass particles suppress growth of small-scale structures by washing out the corresponding density fluctuations. And while keV-scale sterile neutrinos would still be allowed by cosmological models, due to the fact that they become non-relativistic fast, eV-scale sterile neutrinos still remain largely dis-

favored [32]. The relevant observable usually quoted in cosmology is $m^{eff}_{sterile}$, which is related to the standard sterile neutrino mass $m^{thermal}_{sterile}$ [4] through,

$$m^{eff}_{sterile} = \left(\Delta N_{eff}\right)^{3/4} m^{thermal}_{sterile} . \tag{1.7}$$

The effective sterile neutrino mass adds an additional parameter to CMB background anisotropies and in the Planck analysis [34] is constrained to be < 10 eV, to cut the parameter space where neutrinos would behave as dark matter. The reason behind this, is that sterile neutrinos of the eV scale can add a hot dark matter component in the Universe, which is inconsistent with observations [35].

The current limits [34] for N_{eff} and $m^{eff}_{sterile}$ are

$$N_{eff} < 3.7 \text{ and } m^{eff}_{sterile} < 0.52\,\text{eV} \text{ , 95\% C.L.}. \tag{1.8}$$

Although cosmological data disfavor the existence of a sterile neutrino, there is some minor tension in cosmological models that still leaves room for the RAA neutrino to exist [34]. The resolution to the light sterile neutrino problem can come from a model independent measurement, such as the tritium β-decay in the KATRIN experiment, where the sterile neutrino mass and its mixing to the active neutrino can be resolved only through kinematics.

1.2.4 Sterile Neutrinos in β-decay

In neutrino mass β-decay experiments such as KATRIN, the sterile neutrino can modify the electron rate of the decay. The decay rate, commonly refered to as the electron differential spectrum, has been shown to be

$$\frac{d\Gamma}{dE} = C \cdot F(E, Z=2) p\,(E + m_e)\,(E_0 - E) \sum_i |U_{ei}|^2 \sqrt{(E_0 - E)^2 - m^2_{\nu_i}}, \tag{1.9}$$

where E is the energy and p the momentum of the electron, E_0 the endpoint energy, m_e the mass of the electron, m_{ν_i} the neutrino masses and $|U_{ei}|^2$ their corresponding mixing amplitude, $F(E, Z=2)$ the relativistic Fermi function and C a constant. The constant is given as

$$C = \frac{G_F^2}{2\pi^3} \cos\theta_c{}^2 |M|, \tag{1.10}$$

[4] The "thermal" here denotes that the sterile neutrino becomes thermalized as is the case with other particles. The distinction is made because there are other models to include sterile neutrinos in cosmology, which are not discussed here [33].

with G_F denoting the Fermi constant, θ_c the Cabbibo angle, and M the energy-independent nuclear transition matrix element. The Fermi function $F(E,Z)$ encodes the interaction of the outgoing electron with the daughter nucleus. The observable in KATRIN (and generally in β-decay experiments) is not the neutrino mass eigenstate m_ν, but an effective neutrino mass,

$$m_{\nu_e}^2 = \sum_i |U_{ei}|^2 \cdot m_{\nu_i}^2 . \tag{1.11}$$

This approximation is motivated by the fact that the difference of the various mass eigenstates is too small ($\sim 10^{-5}$ eV^2) to be resolved with such an experiment [36].

In the case of an additional heavier mass state, as in the case of a sterile neutrino, the difference in mass can be resolved and as such, the differential spectrum becomes,

$$\frac{d\Gamma}{dE} = \cos\theta^2 \frac{d\Gamma}{dE}(m_{\nu_e}) + \sin\theta^2 \frac{d\Gamma}{dE}(m_s), \tag{1.12}$$

with θ being the mixing angle of active and sterile states and m_s the additional mass [37].

The effect of an active and sterile neutrino mass on the spectrum is shown in figure 1.3. The addition of a sterile neutrino produces a "kink" on the spectrum. This kink comes from the overlap of the two constituents of equation 1.12. A spectrum containing a positive sterile neutrino mass component would take the analogous energy away from the electron, as is the case with the effective active neutrino mass. So in this case, we effectively have two different spectra, each having their endpoint shifted by the respective mass. The resulting beta-spectrum is the sum of these two spectra and has a kink at the point where these overlap. In fact, this is also the case for the different active neutrino mass eigenstates, but the kink is too small to be resolved. In figure 1.3, the kink is pronounced because of the unusually big mixing $\sin\theta$ ($\sim$0.3), used for clarity reasons.

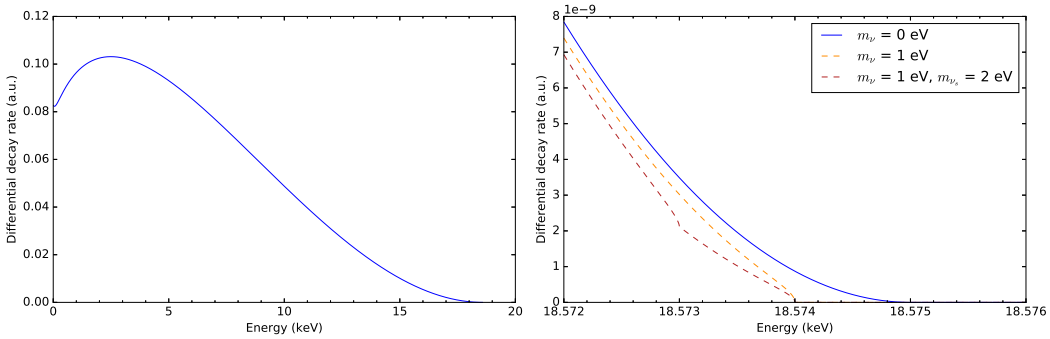

Figure 1.3: *left:* The differential spectrum of electrons in β-decay. *right:* The region near the endpoint of the spectrum is distorted analog to the neutrino mass. In the case of an additional sterile neutrino mass eigenstate we can see the characteristic "kink" signature on the spectrum.

Chapter 2

The KATRIN Experiment

The KArlsruhe TRItium Neutrino experiment (KATRIN) has been designed to determine the effective mass of the electron anti-neutrino with an unprecedented sensitivity of 200 meV/c^2 at 90% C.L., using electrons from tritium β-decay [38]. There are three main reasons why KATRIN uses tritium to measure the electron anti-neutrino mass. Tritium β-decay

$$T_2 \rightarrow THe^+ + e + \bar{\nu}_e \tag{2.1}$$

is super-allowed, it has a half-life of 12.3 years and it has one of the lowest spectrum endpoint energies at 18.6 keV. A super-allowed transition and a short half-life, mean that the decay happens very fast, giving us higher electron rates. In addition to high rates, the endpoint energy of tritium β-decay is low enough to search for a neutrino signature, which is in the range of eV.

2.1 Experimental Challenges

For KATRIN to surpass its predecessors and determine the neutrino mass with great precision, four conditions have to be fulfilled. These are:

1. High signal rate
2. High energy resolution
3. Low background rate
4. Spectral shape knowledge

The high signal and low background rate conditions can be understood intuitively. Only a very small fraction of the electrons have energies in the endpoint region and to have sufficient statistics, a high rate and a very small background are essential. In order to resolve the endpoint shift, induced by the neutrino mass, an excellent (~1 eV) energy resolution is needed. In our case, KATRIN has to be able to distinguish a spectrum containing a sterile neutrino and one without. If the

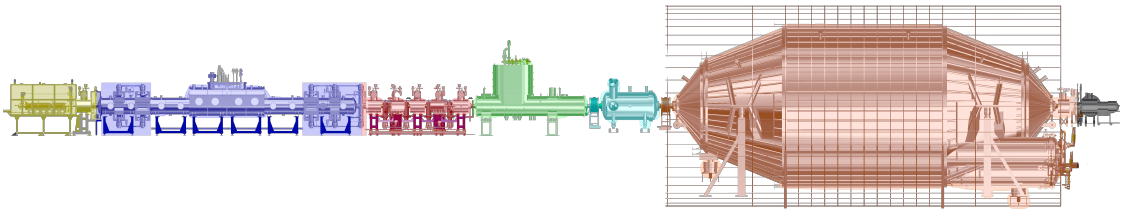

Figure 2.1: Schematic overview of the 70m KATRIN beamline: *yellow:* Rear section, *blue:* Windowless Gaseous Tritium Source (WGTS), *red:* Differential Pumping Section (DPS), *green:* Cryogenic Pumping Section (CPS), *light blue:* Pre-spectrometer, *orange:* Main spectrometer, and *black:* Focal Plane Detector (FPD). Taken from [39].

sterile and active masses lie close together and the mixing is weak, the two spectra look very similar. Depending on the background rate, they could be almost indistinguishable. This calls for advanced experimental techniques and robust analysis methods. As far as analysis is concerned, this problem will be adressed in the final chapter, where it is shown, that by measuring a wider region around the endpoint, we get more spectral information and thus an improved sensitivity.

In the next section, the experimental setup of KATRIN will be presented, where it is made clear how KATRIN surpasses the experimental challenges for a neutrino mass measurement in the sub-eV range.

2.2 Experimental Setup

The full ~ 70 meter long setup is depicted in 2.1.

As mentioned before, the experiment is motivated by a direct measurement of the neutrino mass, and thus relies on a high luminosity source and a good energy resolution. The resolution of KATRIN is achieved with the Magnetic Adiabatic Collimation with Electrostatic filter (MAC-E filter) technique, the working principle of which is depicted in figure 2.2.

The MAC-E Filter

Two superconducting solenoids on both sides of the spectrometer create an axially symmetric magnetic field. The magnetic field that is induced, spans through

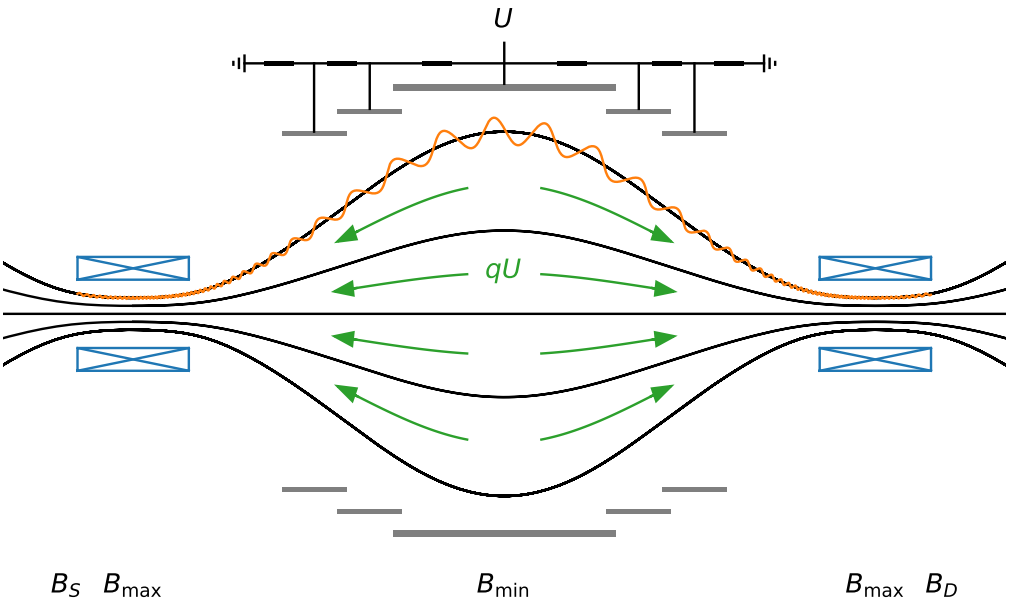

Figure 2.2: The MAC-E Filter working principle. The magnetic fields from the two superconducting solenoids B_{max} are tuned higher than the magnetic fields at the source side B_S and at the detector side B_D. The electrons (*orange*) traverse the magnetic field lines (*black*), while in cyclotron motion around them. As they pass the analyzing plane, they are subjected to an electric field qU. The ones with energy higher than the electrostatic potential reach the detector. Figure taken from [39].

the whole volume of the spectrometer, with the field in the middle of it being several orders of magnitude lower than the one in the magnets. The electrons coming from the source go through the spectrometer and do two types motion. One motion parallel to the magnetic field lines, and one cyclotron motion around them. The momentum of the electron p can be always factorized in a parallel, $p_{\parallel}$, and perpendicular, $p_{\perp}$, component. As the electron flies through the spectrometer, its perpendicular component is transformed to a parallel one by the magnetic field gradient. Because the change in the magnetic field strength is small during one period of the electron's cyclotron motion, this transformation is adiabatic. The adiabaticity makes the electron's magnetic moment

$$\mu = \frac{p_{\perp}^2}{2mB} = \text{const.}, \tag{2.2}$$

where m is the mass of the electron and B the magnetic field. This implies that when the magnetic field is minimum, the parallel component of the momentum,

$p_{\parallel}$ will be maximum. At this point, which corresponds almost to the middle of the spectrometer, an electric field is applied that acts as a barrier for the electrons. As such, only the electrons with energy high enough to bypass this electrostatic potential reach the detector, whereas the rest fly back to the source.

By changing the strength of this electric field, we can control the amount of electrons reaching the detector. This results in the so called "integral measurement", because we measure all the electrons with energies higher than a certain value.

The high luminosity rests to the fact, that there is a high acceptance angle for electrons that come in the spectrometer. As a matter of fact, electrons that come with a greater incident angle, are the ones that scattered the most in the source before going into the spectrometer. These are also the electrons that are more influenced by systematic effects in the source. As we do not want electrons that have scattered a lot in the source reaching the detector, the magnetic field in the source B_s is tuned lower than the maximum magnetic field B_{max}. The maximum acceptance angle, θ_{max}, is then

$$\theta_{max} = \arcsin\sqrt{\frac{B_S}{B_{max}}}. \tag{2.3}$$

The present field configuration in KATRIN is $B_S = 2.52$ T and $B_{max} = 4.2$ T, which leads to a maximum acceptance angle of $\theta_{max} = 50.8°$.

The MAC-E Filter Transmission Function

The resolution of the MAC-E filter is based on how well the parallel energy component can represent the total energy of the electrons at the moment when the electrostatic potential is applied, or in other words, on how efficient is the adiabatic transformation of the perpendicular momentum component. The relation for the resolution

$$\frac{\Delta E}{E} = \frac{B_{min}}{B_{max}}, \tag{2.4}$$

where B_{min} is the minimum magnetic field on the analyzing plane, shows how we should pick the field strengths to achieve the best possible energy resolution. However, as the flux

$$\Phi = \int B \mathrm{d}A = B_S \times A_S = B_{ana} \times A_{ana} = \text{const.}, \tag{2.5}$$

with A_S the cross-section of the source, A_{ana} of the analyzing plane, and $B_{ana} = B_{min}$, is conserved, we see that the smallness of the resolution actually depends on how big A_{ana} i.e. the spectrometer is. This comes from the fact, that a magnetic field cannot be arbitrarily small, and as such the cross sectional area in the analyzing

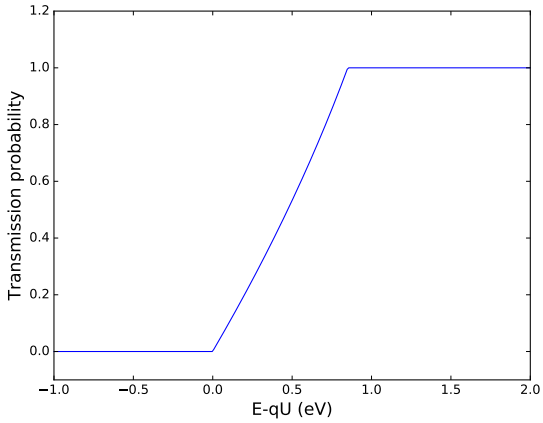

Figure 2.3: Transmission function of the MAC-E filter of KATRIN. The width of the step corresponds to the nominal energy resolution at 18.6 keV of ΔE = 0.93 eV.

plane has to be correspondingly large to compensate. For the first measurement phase, with $B_{ana} = 6$ G[1], at an energy of 18.6 keV, the energy resolution was ΔE = 2.66 eV.

The ideal MAC-E filter has a response,

$$T(qU,E) = \begin{cases} 0 & E < qU \\ \dfrac{1-\sqrt{1-\frac{B_S}{B_{ana}}\frac{E-qU}{E}\frac{2}{\gamma+1}}}{1-\sqrt{1-\frac{B_S}{B_{max}}}} & qU \le E \le qU\frac{B_{max}}{B_{max}-B_{ana}} \\ 1 & \text{otherwise} \end{cases} \tag{2.6}$$

which we call transmission function. Here, $\gamma = E/m_e + 1$ is just a relativistic factor. The transmission function dictates the probability that an electron can pass the electrostatic barrier. Its shape depends on the resolution of the MAC-E filter and the acceptance angle. The transmission function of KATRIN for the design energy resolution of ΔE = 0.93 EV, is shown in figure 2.3.

The MAC-E Filter technology was tested and used by the Mainz [40] and Troitsk [41] experiments, of which the latter gives the current effective electron antineutrino mass upper limit,

$$m_{\bar{\nu}_e} < 2.05\,\text{eV}. \quad 95\%\ \text{C.L. (Feldman-Cousins).} \tag{2.7}$$

[1] 1 G = 10^{-4} T

The KATRIN Beamline

In the following, the building blocks of KATRIN will be briefly discussed.

The Rear Section

The rear section closes the ultra high vacuum system of the WGTS. While its main function is to enclose the tritium gas, it also houses instruments to monitor the properties of the gas inside the source [42].

WGTS

The WGTS is where the tritium is decaying and where most of the relevant systematic effects take place. It is a highly luminous and stable tritium source, being injected by ultra-cold molecular tritium gas, with isotopic purity ~95%. This results in about 10^{11} β-decays, or electrons, per second.

The main systematic uncertainty that arizes in the WGTS is on the column density ρd; that is, the number of molecules per cross sectional area. For the final tritium measurements of KATRIN, its value will be tuned to 5×10^{17} molecules/cm^2 [38].

DPS and CPS

The transport section is divided in the Differential Pumping Section (DPS) and the Cryogenic Pumping Section (CPS). The pumping section is deticated to shrinking the ion flow in the beamline, thus reducing this additional background factor. In the DPS, turbomolecular pumps reduce the tritium gas and ions by a factor of $\sim 10^{-4}$ [43]. In the CPS almost all the remaining tritium is adsorbed on the surfaces of the beam tube, which are coated with a pre-condensed argon layer. Using this technique, the tritium flow can be further reduced by 7 orders of magnitude [44], thus ensuring that no ions can reach the spectrometers.

The Pre-spectrometer and the Main Spectrometer

Both spectrometers work based on the MAC-E principle. The pre-spectrometer serves as a first filter for electrons, to supress the rate and to let only the high-energetic electrons pass through. By setting the electric potential ~300 V below the endpoint energy, the pre-spectrometer can already reduce the incoming electron flux by 6 orders of magnitude.

The relevant for the neutrino mass measurement electrons pass the pre-spectrometer and through two superconducting transport magnets, and reach the

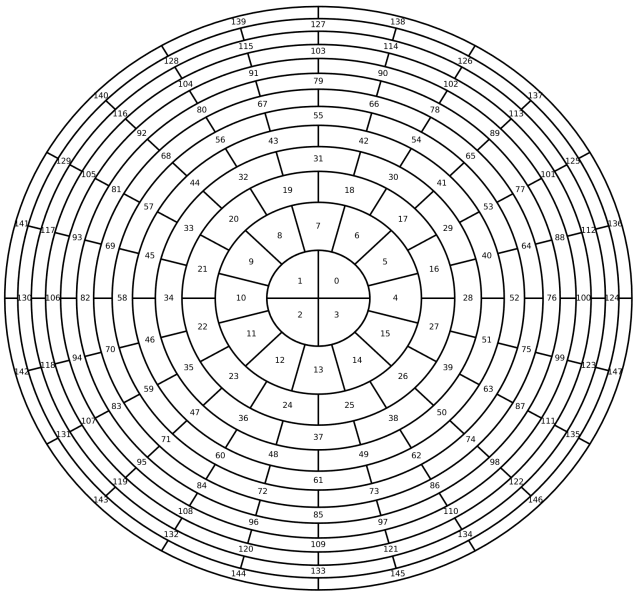

Figure 2.4: The KATRIN focal plane detector. The radial segmentation in pixels helps identify inhomogeneities in the beamline.

main spectrometer. The size of the main spectrometer is what makes KATRIN competitive in the neutrino mass search, with its design sensitivity being almost five times better than older MAC-E filters [38].

Focal Plane Detector

The electrons that pass the main spectrometer arrive on the FPD. It consists of 148 pixels and is segmented as shown in figure 2.4. It is based on the silicon p-i-n array technology and has an energy resolution of 1.52±0.01keV (FWHM) per pixel [45]. The segmentation allows us to check for inhomogeneities in the background, magnetic fields and the source.

2.3 Modelling the Spectrum

To get from the differential spectrum in equation 1.9 to the integrated spectrum that KATRIN measures, the differential rate has to be integrated together with the response function of the experiment. If the electrons would not scatter in the source, this would just be the transmission function 2.6.

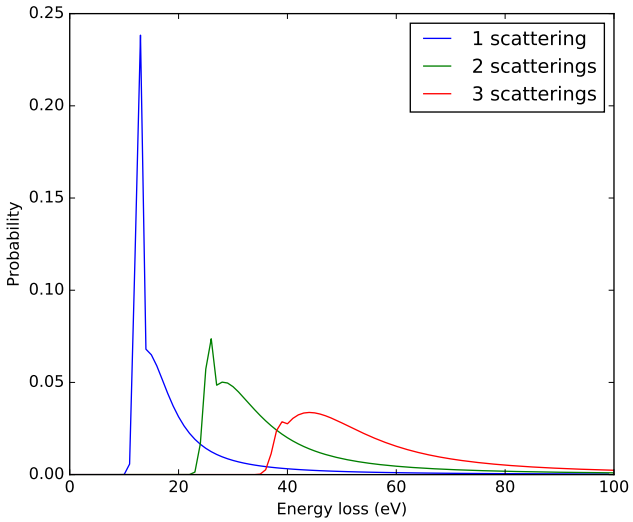

Figure 2.5: The energy loss function for up to three scatterings. The loss probability for each scattering is plotted against the energy. Each additional order of scattering corresponds to an additional convolution of the function with itself.

To take scatterings in the source into account, the transmission has to be convoluted with the energy loss function, that is, the function that dictates the energy an electron loses after a certain amount of scatterings.

The energy loss function for one scattering,

$$f_1(\epsilon) = \begin{cases} A_1 \exp -2\frac{(\epsilon-\epsilon_1)^2}{\omega_1^2} & \epsilon < \epsilon_c \\ A_2 \cdot \frac{\omega_2^2}{\omega_2^2+4(\epsilon-\epsilon_2)^2} & \epsilon \geq \epsilon_c \end{cases} \tag{2.8}$$

consists of a Gaussian part, with mean ϵ_1 and variance ω_1, and a Lorentzian part, with mean ϵ_2 and variance ω_2. The energy loss function for n scatterings is given by the convolution of the function with itself, n-times. In the case of no scatterings, expression 2.8, is reduced to just a Dirac delta function,

$$f_0(\epsilon) = \delta(\epsilon). \tag{2.9}$$

The energy loss functions up to three scatterings, are depicted in figure 2.5.

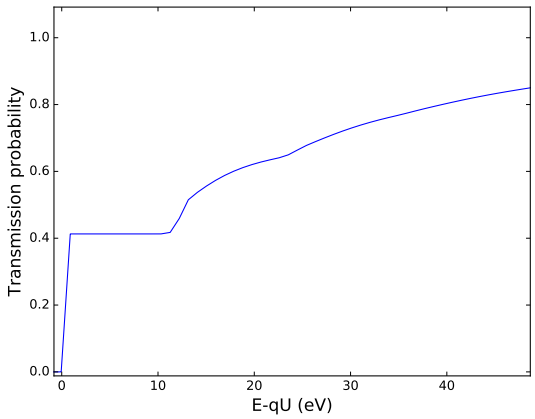

Figure 2.6: The response function of KATRIN. The form of the function is derived by taking scattering of electrons in the source into account. In principle, the response function is the transmission of the MAC-E filter, weighted by the probability of an n-fold scattering to take place, and the n-fold convolution of the energy loss function. The first step at ~10 eV below the endpoint denotes the first scattering.

The transmission function is weighted by the probability of n scatterings P_n and the n-fold convolution of the energy loss f_n to give the response function,

$$R(qU,E) = T(qU,E) \cdot \sum_{i=0}^{n} P_n f_n, \tag{2.10}$$

where P_i is the probability for i scatterings to take place. The impact of the energy loss function is described in section 3.3.

The response function is shown in figure 2.6. We see that electrons will leave the source unscattered with 41% probability. Each additional scattering produces another distortion, deeper into the spectrum.

The resulting integral spectrum is then,

$$I(qU) = \int_{qU}^{E_0} \frac{\mathrm{d}\Gamma}{\mathrm{d}E} \cdot R(qU,E)\mathrm{d}E, \tag{2.11}$$

where the integral goes from the retarding energy at a point, to the endpoint of the spectrum E_0. The model signal $\Gamma(qU)$ is completed by multiplying the integral spectrum with a constant normalization factor N and adding a background rate B,

$$\Gamma(qU) = N \cdot I(qU) + B. \tag{2.12}$$

Chapter 3

The First Tritium Measurement Campaign

In June 2018 KATRIN took the first measurements of tritium beta-decay by injecting D_2 gas with 1% DT into the source. The concentration of tritium was fairly low, but served as a starting point for the KATRIN experiment. These measurements, which we call "First Tritium" (FT), were done mainly to demonstrate the functionality and stability of the whole setup and were not intended for measuring the mass of the neutrino. The observable in question was the effective endpoint of the tritium beta spectrum. Important was to assure the stability of the endpoint, thus providing a justification for the numerical methods used in the upcoming analysis. This first measurement period was very important for the study of sterile neutrinos, as the low tritium purity allowed us to measure 1600 eV below the physical endpoint of the tritium β-spectrum, an energy scale that normally has such high electron rates, that the detector cannot handle. This allowed for a more extended search of a spectral distortion.

In the following, we will present our analysis methods, data handling techniques, and the results of the light sterile neutrino analysis with the FT data.

3.1 Analysis Methods

For the analysis we use the analysis tool "Fitrium" [39]. Fitrium includes a model of the tritium β-decay and the KATRIN apparatus, an application for Monte Carlo data generation and is linked to the software "Fitness Studio", with which it can also fit the data. Both softwares are developed at the MPP, mainly by C.Karl and M.Slezák. In the framework of this thesis, Fitrium was extended to also accomodate a sterile neutrino. For our analysis, we used the method of significance testing, constructing frequentist confidence intervals.

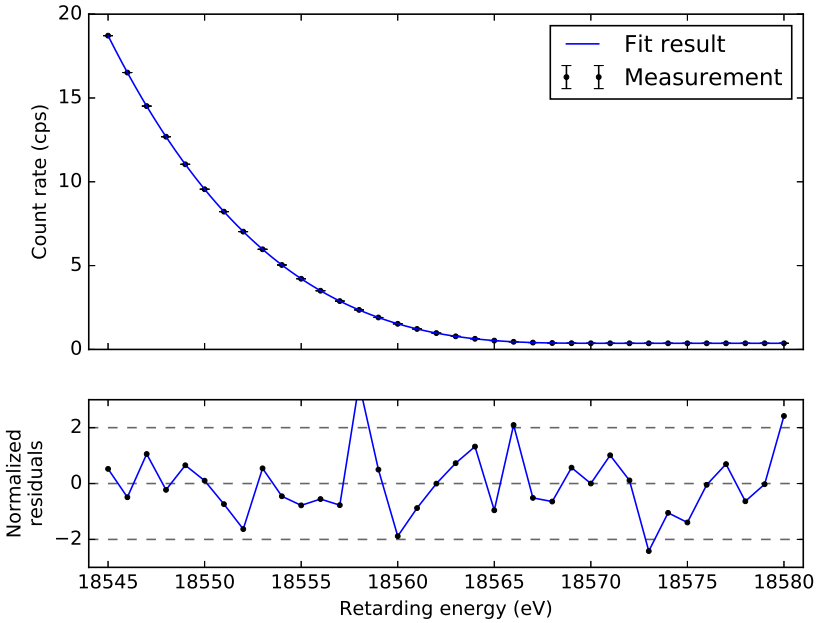

Figure 3.1: A fit of a fluctuating Monte Carlo dataset, simulating 3 years of KATRIN data with zero neutrino mass.

We assume that each decay is independent of one another, and for each point in the spectrum we use a Poissonian likelihood of the form

$$P(x_i \mid N) = e^{x_i} \frac{x_i^N}{N!}, \tag{3.1}$$

where N is the total number of counts and $x_i = x(E_0, B, N, m_\nu)$ denotes the underlying model. Here, E_0 is the physical endpoint of the β-spectrum, B the background rate, N the overall amplitude, which we call the normalization, and m_ν the neutrino mass. The final likelihood is then the product of each indiviual likelihood, as we also take each measurement to be independent from each other.

For our analysis, we fix the neutrino mass to zero and fit the other three parameters. A fit of Monte-Carlo data in the last 30 eV close to the endpoint is shown in 3.1.

3.1.1 The Covariance Matrix Approach

To include systematics in the analysis we used the covariance matrix method [46]. In this method, we minimize a χ^2-function of the form

$$\chi^2\left(\vec{x}_i \mid \vec{N}\right) = (\vec{x}_i - \vec{N})^T V^{-1} (\vec{x}_i - \vec{N}), \tag{3.2}$$

where $\vec{x_i}$ and $\vec{N}$ are vectors containing the model prediction and counts for the whole dataset and V is the covariance matrix, which encodes the correlated and uncorrelated uncertainties of the systematic effects. This method is viable, because for large rates the poissonian likelihood resembles the normal distribution, and then we can relate our likelihood 3.1 to 3.2 as

$$\chi^2\left(\vec{x}_i \mid \vec{N}\right) = -2 \ln P\left(\vec{x}_i \mid \vec{N}\right). \tag{3.3}$$

The covariance matrix approach of determining systematic effects can be used only if the data is normally distributed and entails the following steps. First, Monte-Carlo datasets are generated ($\sim 10^3$), in which the systematic parameter in question is varied according to a given distribution. Then, for each point the covariance of the rates $\vec{R_i}$ is calculated according to

$$\mathrm{cov}\left(R_i, R_j\right) = \frac{1}{N_{spectra}} \sum_{k=1}^{N_{spectra}} (R_{i,k} - \langle \vec{R_i} \rangle)(R_{j,k} - \langle \vec{R_j} \rangle), \tag{3.4}$$

where $N_{spectra}$ is the number of spectra generated and $\langle \vec{R_i} \rangle$ is the expectation value of the rate at each point. Finally, we construct the covariance matrix of systematic effects as

$$V_{sys} = \begin{pmatrix} \mathrm{cov}(R_0, R_0) & \mathrm{cov}(R_0, R_1) & \dots & \mathrm{cov}(R_0, R_n) \\ \mathrm{cov}(R_1, R_0) & \mathrm{cov}(R_1, R_1) & & \vdots \\ \vdots & & \ddots & \vdots \\ \mathrm{cov}(R_n, R_0) & \dots & \dots & \mathrm{cov}(R_n, R_n) \end{pmatrix}. \tag{3.5}$$

For each systematic effect we want to include in our analysis, we construct such a matrix. To include statistical uncertainty, we construct a diagonal matrix V_{stat}, the same dimension as V_{sys}. These diagonal entries should be equal to the variance at each point σ^2, which corresponds to the statistical error square.

The covariance matrix we then use in 3.2 is the sum of all those matrices,

$$V = \sum_s V_{sys,s} + V_{stat}, \tag{3.6}$$

where s runs over the total number of systematic effects included in the analysis.

Table 3.1: Values of $\Delta\chi^2$ corresponding to a Confidence Level and to a number of standard deviations. These values are valid in the case of two estimated parameters.

C.L.	σ	$\Delta\chi^2$
68.27%	1	2.3
90%	1.645	4.61
95.45%	2	6.18
99.73%	3	9.21

3.1.2 χ^2 Significance Testing

To compute the sensitivity of KATRIN to sterile neutrinos, we used the standard procedure of a χ^2 test. We first construct our likelihood with the mass squared m_s^2 of the sterile neutrino and its mixing $\sin^2\theta$ with the active one. We vary the parameters by hand, and for each point in the m_s^2 - $\sin^2\theta$ plane, we fit the usual parameters. Then, to construct the 90% C.L. belt, we calculate the $\Delta\chi^2$ as

$$\Delta\chi^2 = \chi^2\left(\vec{x}_i \mid \vec{N}\right) - \chi^2_{best}\left(\vec{x}_i \mid \vec{N}\right) < 4.61\,, \tag{3.7}$$

where the equivalence of $\Delta\chi^2$ values to significance levels is shown in table 3.1.

The resulting curve is a so called exclusion curve, defining the parameter space we can exclude with the given C.L. (all points with $\Delta\chi^2 > 4.61$). In this thesis, the excluded space is the space to the right of the curves i.e. the area indicating larger values for the mass and mixing angle, than the ones defined by the curve.

In table 3.2 the design parameters of KATRIN are summarized. By adding the systematics stated in the design report [38], we reproduced to a good degree the sensitivity from older studies as seen in figure 3.2.

3.2 Data Handling

Pixel Combination

The usual way to fit a spectrum would be to fit pixel dependent parameters, such as the normalization and background rate, per pixel, while fitting the endpoint, which

Table 3.2: Table listing the settings of KATRIN for the neutrino mass and FT measurement campaign.

Parameter name	Nominal value	First Tritium
ρd	$5{\times}10^{17}\mathrm{m}^{-2}$	$4.5{\times}10^{17}\mathrm{m}^{-2}$
B_s	3.6T	2.52T
B_{max}	6T	4.2T
B_{ana}	$3{\times}10^{-4}$T	$6{\times}10^{-4}$T
Detector efficiency	95%	95%
Tritium purity	95%	0.5%

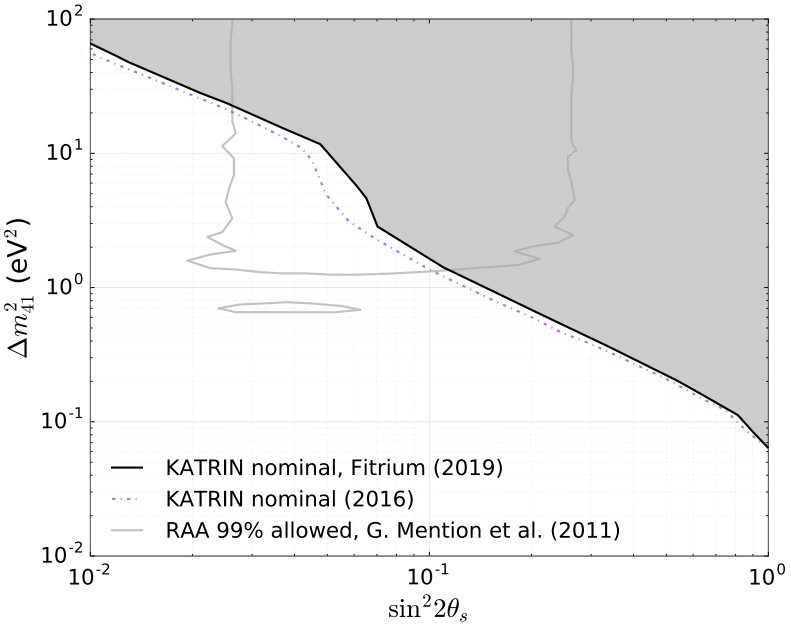

Figure 3.2: Nominal KATRIN sensitivity study. The nominal KATRIN curve is adapted from [47]. The curve (*black*) produced by Fitrium agrees to a very good level. The excluded parameter space is the grey area above the curve. For illustration purposes, the allowed region of the original RAA is shown as the area enclosed by the grey line.

is a physical parameter, independently. However, such a fit would be too time-consuming and greatly complexes the sterile neutrino analysis, as we need at least 200 evaluations of the χ^2 function to produce a low resolution exclusion curve. For this, we treated the whole detector as one pixel, averaging the parameters that can be pixel-dependent, such as the normalization and background. This procedure, which we call a "uniform fit", greatly speeds up the fitting procedure, while losing all the per-pixel information. Although the very essence of the FPD segmentation was to fit for all pixel parameters independently, due to homogeneity during FT, we deemed that averaging pixel dependent parameters would not induce systematic shifts, and thus proceeded with the uniform fit approximation.

Run Combination

To ensure stability of the system, KATRIN does not take data continuously, but rather does smaller measurements that are to be combined at a later time. One full integral measurement of the spectrum is called a "run", and from the First Tritium analysis, we picked 27 of those runs that lasted for three hours each (~3.4 days of measuring time in total). One point in the spectrum corresponds to a retarding potential value. This measurement point is called a "subrun", and the stability of the high voltage value at each measurement point plays a significant role in the process of combining runs.

To use the covariance matrix method described in section 3.1.1, and to make the analysis faster, we have to combine runs with the exact same measurement point position. As the high voltage may have a small drift from the input value, the actual qU values are not the same for every independent measurement. The bins used for the analysis with a covariance matrix are then defined by the average qU values of the combined runs. This process, called "stacking", introduces a mass shift error of $\Delta m^2 = -2\sigma^2$ depending on the variance σ^2 of the stacked points. This effect was shown to be irrelevant for the statistics of the FT measurements [39].

3.3 Systematics Budget

A uniform fit of the 27 three-hour runs stacked is shown in figure 3.3, with and without including systematics.

The resulting χ^2 over degrees of freedom is 2.61 in the statistics only case and 0.74 when we include systematics. The degrees of freedom for a fit are defined as the number of data points subtracted by the number of free parameters. The number of degrees of freedom coincides with the expectation value of the χ^2 if the measurements follow a Gaussian distribution. So a χ^2 value close to one is desirable. It is easy to see that our model fits the data well in both cases, but becomes significantly better if we include systematics. This section is deticated to

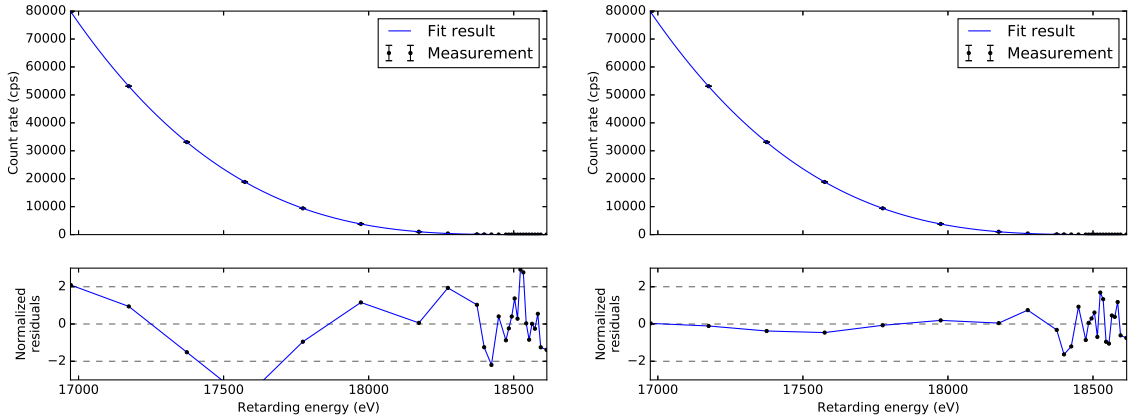

(a) (b)

Figure 3.3: Fit of the combined 27 three-hour runs. (a) shows a fit with statistical uncertainty only. (b) shows one including systematics. The bottom plot in each figure shows the residuals normalized to standard deviations.

the breakdown of systematic effects included in the analysis, and the final results for the light sterile neutrino analysis of the FT data.

Column Density ρd

The column density ρd is one of the main systematic effects, as its product with the total inelastic scattering cross section σ is proportional to the scattering probabilities. Its stability ensures that there are no significant distortions in the shape of the spectrum. The cross section has an associated uncertainty of 2% [48]. In FT, ρd was treated with a systematic error of 2-3%. The monitoring of the column density is achieved with various techniques such as by the gas throughput and pressure [49]. The definitive value for the column density will be provided by an electron gun, used to measure directly $\rho d\sigma$ by shooting monoenergetic electrons through the WTGS and onto the detector. The ρd stability requirement for the nominal KATRIN operation is 0.2%.

In figure 3.4, a $\rho d\sigma$ fit on simulated electron gun data with Fitrium is shown. The electron gun energy was fixed at 18575 eV.

Energy Loss Function

As electrons travel to reach the detector, they can scatter and lose energy in the process. This loss of energy is modelled with an energy loss function as in equation 2.8, and the uncertainties on its parameters are taken from [50]. The energy loss function plays a great role in the experiment, as it dictates the way the transmission of the electrons is distorted due to taking part in inelastic collisions in the source. The energy loss determines the shape of the response function. For this reason, the shape of the energy loss function has to be known with great precision for both the neutrino mass measurement, and the sterile neutrino sensitivity.

The shape of the energy loss function can be inferred from measurements of an electron gun spectrum for different column densities in the source. The exact procedure is described in [38].

Final States Distribution (FSD)

As T_2 molecules decay, the nuclear recoil forces them to land in different ro-vibrational final states with a distribution of excitation energies as seen in figure 3.5. This modifies the spectrum, as the available energy for an electron becomes less. The distributions for these states were given in [51]. As seen in figure 3.5, the FSD is divided in mainly two parts, the first being a sharp peak indicating the

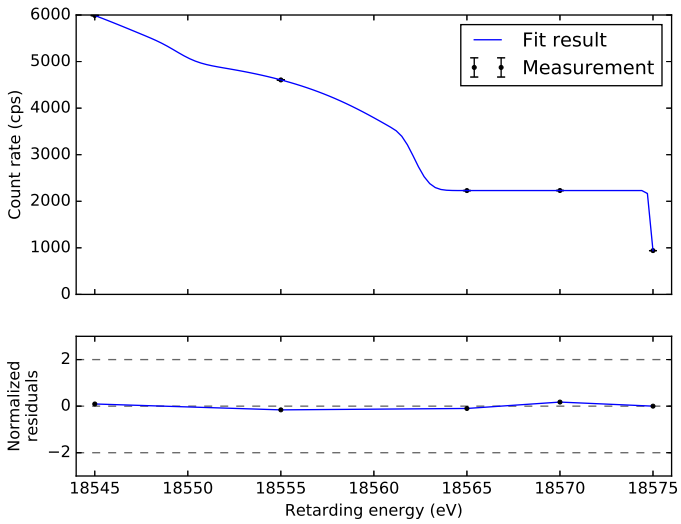

Figure 3.4: A fit on simulated electron gun data. Each additional scattering process taking place in the source adds a bump deeper in the spectrum.

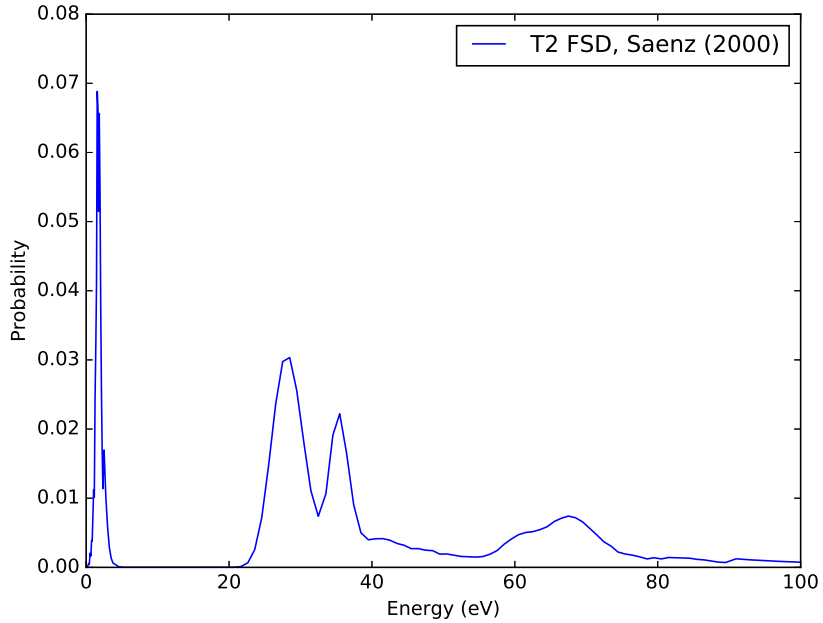

Figure 3.5: The FSD data for the T_2 molecule going into Fitrium. In the distribution the first sharp peak indicates the ground states, and all the structures on the right belong to excited states.

ro-vibrational excitation energy probability distribution of the electronic ground state, and the second showing the probability for the electronic excited states.

The systematic uncertainty of the FSD comes mainly from the normalization of the ground to excited states. However, the excited states probability is not so well understood, and the total probability has to be conserved. For this reason, we assumed in FT a overall normalization uncertainty of 1% and an additional uncertainty of 2-3% for the variance of the whole FSD.

Magnetic fields

As the parameters that dictate the incident electron angle in the spectrometer, the adiabaticity of the MAC-E filter and most importantly, the resolution of KATRIN, uncertainties on the strength of the magnetic fields play a great role. This systematic is dependent on the hardware and in the design report has an accuracy

requirement of 0.2% for all three magnetic fields, B_{ana}, B_S, and B_{max}. For the FT, the systematic uncertainties were derived from simulations, and were 1%, 2.5%, and 0.2% for B_{ana}, B_S, and B_{max}, respectively.

Isotopologue Concentration Fluctuations

Tritium can come in the source in the form of T_2, HT and DT. In FT the source of electrons was DT, which consisted almost the 1% of the total gas (mainly D_2). Fluctuations in the activity of the DT isopologue can induce spectral distortions. This means that the stability of its concentration was crucial to the analysis that followed. The concentration, as well as the errors on it, are given through laser Raman spectroscopy [52]. As the concentration of DT was very small, it could not be measured very accurately. As such, the measured mean value of the DT concentration was fluctuating during FT. The fluctuations during the 27 analyzed runs are shown in the evolution of the DT concentration in figure 3.6.

We see that the concentration can change by more than ±0.2% relative to the mean value. In relative, we show the evolution of the column density, as a demonstration of the stability of the KATRIN apparatus. Although these two parameters do not say anything about each other, the difference in measurement precision is made clear. These fluctuations introduced a new systematic to the analysis, as KATRIN was not designed to operate on such small concentrations of tritium.

For the analysis we used the error on the mean as uncertainty, which roughly ranged from 0.05% to 0.18% for the 27 runs. Although the DT fluctuations were the most impactful systematic during FT, any fluctuations of statistical nature will be washed out by measuring longer, so we do not expect such uncertainties in the standard KATRIN operation.

Detection efficiency

After the electrons pass the main spectrometer, they are re-accelerated to reach the detector. For the reconstruction of the integral spectrum, one has to define a certain Region Of Interest (ROI) to get rid of non-tritium events recorded in the detector. What this ROI cut achieves, is the reduction of unneccesary background, created either by processes in the main spectrometer or by hardware-induced noise. The error on the correction stemming from the ROI cut was taken as 0.16% at 1600 eV below the endpoint.

One other major effect in the FPD that is resolved through the ROI cut, is the rejection of pile-up electrons. If two electrons hit on the same pixel at a certain timescale, which the detector cannot resolve, the detector records one event at an

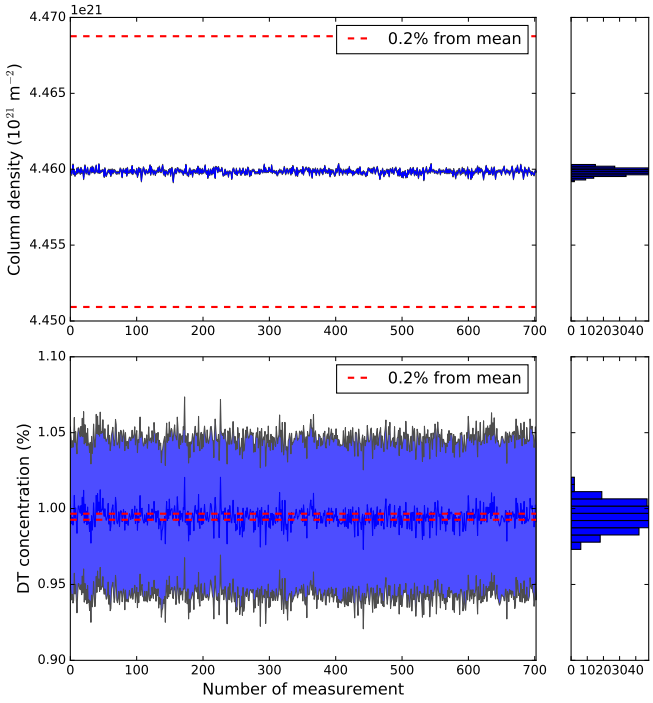

Figure 3.6: The evolution of the column density and DT concentration for the duration of the 27 runs. Although the two parameters cannot really be compared, the fluctuation of the measured mean DT concentration value is made clear.

energy depending on the incident times of the electrons. As pile-up can lead to a loss of an uncertain amount of electrons, the error on its correction was pessimistically fixed to 18%.

Another loss of statistics can come from the backscattering of electrons in the magnet situated at the detector. Although most electrons can scatter back and forth, ultimately reaching the detector, some can go through the main spectrometer again and travel back to the source. The error on the backscattering correction is very small and we do not need to include it in our analysis.

All these effects are taken into account in KATRIN to deliver the detection efficiency of the FPD. The detection efficiency is pixel-, and energy-dependent, and in the FT measurements had a relative correction ranging almost up to 2%. In figure 3.7, we vizualize the energy- and pixel-dependence of the detection efficiency. In this figure the correction on the detection efficiency is plotted for two pixels against the value of the retarding potential.

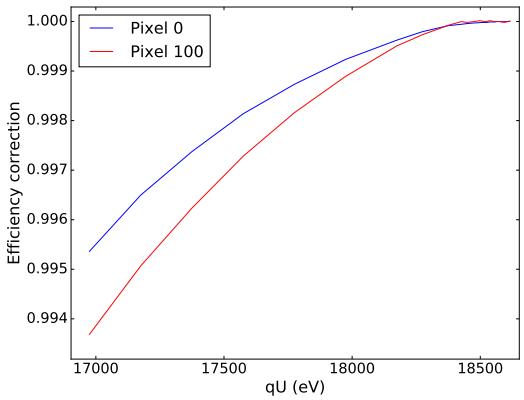

Figure 3.7: The detection efficiency corrections for two pixels. For each measurement point below the endpoint, the ROI window is shifted .

The detection efficiency corrections $\delta_{ROI}(qU)$, $\delta_{PU}(qU)$, were provided by a dedicated group in the collaboration and we calculated the error on the total counts, $\sigma_{N^{corr}}(qU)$, as,

$$\sigma_{N^{corr}}(qU) = \sqrt{(\delta_{ROI}(qU)\cdot\sigma_{ROI})^2 + (\delta_{PU}(qU)\cdot\sigma_{PU})^2} \tag{3.8}$$

$$= \sqrt{\sigma^2_{\delta_{ROI}} + \sigma^2_{\delta_{PU}}}, \tag{3.9}$$

which was dominated by the uncertainties on the pile-up corrections. At qU = E_0-1600, our full range, $\sigma_{N^{corr}}(qU = E_0 - 1600)$ was 0.02%, without taking account the dependence on the different pixels. At qU = E_0-1000, it was $\sigma_{N^{DE}}(qU = E_0 - 1000) = 0.003\%$. We took a pessimistic guess and averaged these uncertainties to yield an 0.01% uncorrelated uncertainty for the whole spectrum in our final analysis.

The systematics included for the analysis of the data are summarized in table 3.3.

Table 3.3: Table listing the values of the different systematics taken into account during the First Tritium measurement campaign.

	Uncertainty
$\rho d\sigma$	3%
FSD normalization	1%
FSD shape	P_{GS}(4%),P_{ES}(18%)
Energy loss fn.	Abdurashitov (D_2)
B_s, B_{max}	2.5%,0.2%
B_{ana}	1%
DT concentration fluct.	0.05-0.18%
Detection efficiency	0.01%

3.4 Results

3.4.1 Comparison of Sensitivity and Exclusion Limit

Having done the preliminary analysis to ensure the stability of the data and the proper function of our model, the next step is to analyze the FT data with respect to light sterile neutrinos.

To demonstrate the robustness of the Fitrium analysis tool, we generated 27 runs with the same slow control parameters as the ones from FT, and drew exclusion curves including all systematics with the real and simulated data. The result, shown in 3.8, indicates not only that Fitrium can simulate data to a great resemblance to reality, which serves as a test for our projected KATRIN sensitivity studies, but also that the FT data were of high quality and did not show unexpected behavior, at least at this level of analysis.

3.4.2 Impact of Individual Systematics

To see how each systematic affects the exclusion, we draw the exclusion, each time with another systematic effect. Figure 3.9a, shows how much impact these uncertainties had in our analysis.

To make the effect of the systematics more clear, we can change our χ^2-test. A way of showing exclusion plots with statistical artifacts is by modifying equation 3.7 as,

$$\Delta\chi^2 = \chi^2\left(\vec{N} \mid \vec{x}_i\right) - \chi^2\left(\vec{N} \mid \vec{x}_i(m_{\nu_s} = 0)\right) < 4.61\,, \tag{3.10}$$

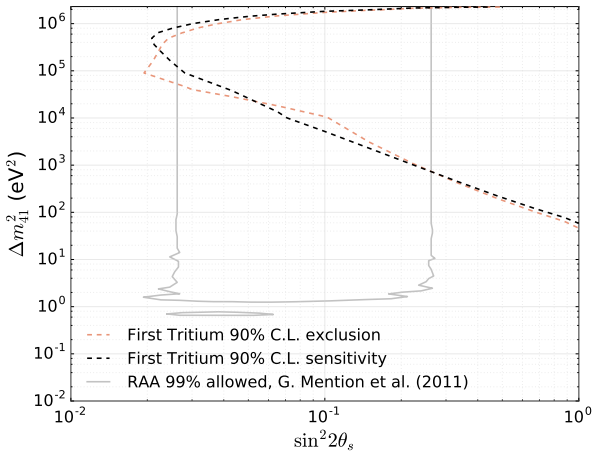

Figure 3.8: The FT exclusion curve is compared with the exclusion produced using simulated FT data. The result serves as a verification for the future sensitivity studies, as far as our software and data quality of KATRIN are concerned.

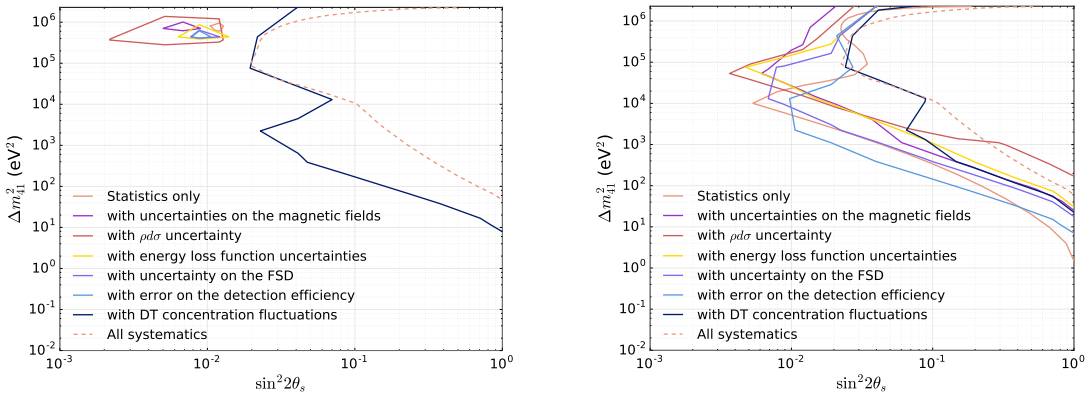

(a) (b)

Figure 3.9: Exclusion curves for the 27 FT runs stacked. Each time we use a different covariance matrix to include a systematic effect in the test. (a) shows the case where the χ^2 is compared to the best fit, and (b) the case compared to the null hypothesis.

where instead of comparing the χ^2 of each point to the best fit, we compare it to the χ^2 value in the absence of sterile neutrino. We call this case the "null hypothesis", as it is the hypothesis we opt to reject. The curves then would show a mild preference towards the best fit value, while retaining a statistically unbiased form. We ought to note here, that this procedure is applied only for presentation reasons and in general is applicable only in the case, where we know that we can exclude the best fit as a possible discovery. We depict this result in 3.9b.

The curve including the uncertainty on the column density and total scattering cross section $\rho d\sigma$ is a bit above the "all systematics" curve, because of numerical effects. For the same reason, the curve with the detection efficiency covariance matrix is below the "statistics only" curve.

The uncertainty on the magnetic fields and on the energy loss function add to the whole of the spectrum. Especially in the regime of higher masses, their effect is more pronounced. The reason for this, lies probably in the fact that the magnetic fields and the energy loss play a role in the transmission and the response function of the experiment, which affect the spectral shape, and in turn the sensitivity on the mass. The uncertainty on the column density seems to have almost the same effect, but it is again getting more pronounced for higher mixing angles. This again, can be attributed to the spectral shape, as the higher mixing angles indicate a more pronounced kink in the spectrum. Our knowledge of the kink signature is directly correlated to the rate at each point, which is proportional to the column density. The last systematic for which we use correlated uncertainties, is the error on the FSD. The excitation energy of the molecules in their final states follow a distribution and do not have an exact value. This worsens the resolution for a very small factor. Indeed, we see that the FSD covariance matrix has an overall effect on the exclusion, except for the region above intermediate masses and mixing angles. This behavior rests to the fact that our model is not made for the region 100 eV and below the endpoint, making the FSD uncertainty in the higher masses regime doubtful.

The uncorrelated systematics we use are for the detection efficiency corrections and the DT concentration fluctuations. Uncorrelated systematics are in general dangerous for analyses looking for a spectral signature, as the absence of correlations implies that the signature in question can be almost always be reconstructed within uncertainties. By including correlations to our systematics, the sought after spectral signature can in principle only be formed due to physical effects. The uncorrelated systematics thus always improve our fit, and simultaneously reduce the sensitivity. This effect is very clear in the First Tritium analysis, as the bin-to-bin uncorrelated uncertainty on the DT concentration completely dominates over all other systematics. As discussed above, this uncertainty is only on the order of 10^{-3}, but still has a much greater impact than, let's say the correlated uncertainty of $\rho d\sigma$, which is of the order of 10^{-2}. Errors on the detection efficiency corrections

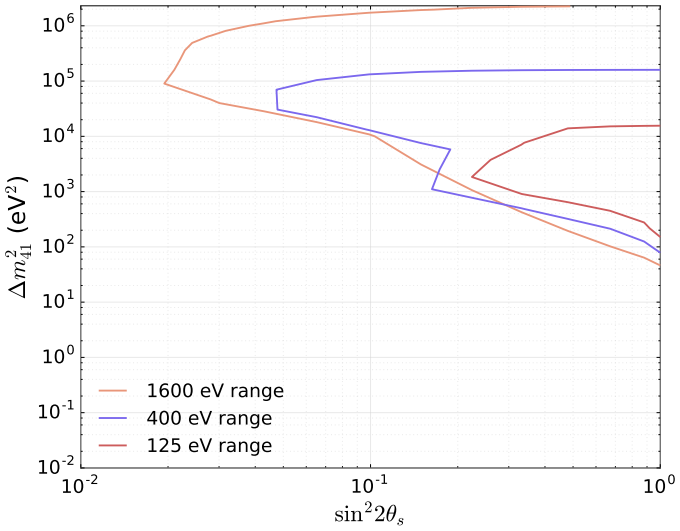

Figure 3.10: The impact of the fitting range in the exclusion curve. We can read that the deeper we scan, the more sensitive we get, even for lower masses.

are on the order of 10^{-4}, and thus do not play a significant role here. However, if we included more statistics in our analysis, also these errors would become significant. The behavior of the curve that is below the "statistics only" curve, could be attributed again to the absence of correlations and the smallness of the error, but this effect was not studied further.

3.4.3 Dependence on Statistics and the Fit Range

The Effect of the Fitting Range

To test the dependence on the fitting range, and to see the limitations of our model, we draw the exclusions including now all systematic effects, but this time varying the fitting range. This study is mainly done in order to validate our analysis at the full 1.6 keV range, with a model that is developed for use at most 100 eV below the endpoint of the beta-spectrum.

The result in 3.10 shows how the fitting range modifies the exclusion curve. The 1600 eV range still is the best option, even though we expect the systematic effects to be less dominant in the smaller fitting ranges. In this case, we can argue that the knowledge of the full spectral shape, which depends on the depth of the scan, plays a greater role than possible systematic uncertainties not included in the analysis.

3.4.4 Comparison to Other Measurements

As a final step, we plot the FT exclusion together with the older exclusions of the Mainz and Troitsk experiments in figure 3.11. Even with a higher background and way lower tritium concentration than the nominal KATRIN operation, FT can compare to the other two β-decay experiments. In the same plot we show a prediction of the exclusion after the first measurement phase of KATRIN that is to take approximately 30 days worth of data time. As the source will contain T_2 gas, the electron rates will be significantly higher, such that above a certain threshold the detector cannot handle. For the curve shown here, we assumed a maximum scan range up to 90 eV below the endpoint. As by having significantly more statistics than FT and statistical fluctuations of the tritium isotopologues will quickly become averaged out, we did not include this systematic in this study.

Already in 30 days of measuring time, KATRIN can exclude a very large part of the parameter space preferred by the reactor antineutrino anomaly. This can be attributed to the high rates due to increased tritium activity and the improved systematic uncertainties. This plot also showcases the importance of KATRIN as a β-decay experiment, as it has the prospects to greatly improve past results.

In the next chapter, we test the limits of KATRIN by computing the sensitivity for the full 3 years of measurement time.

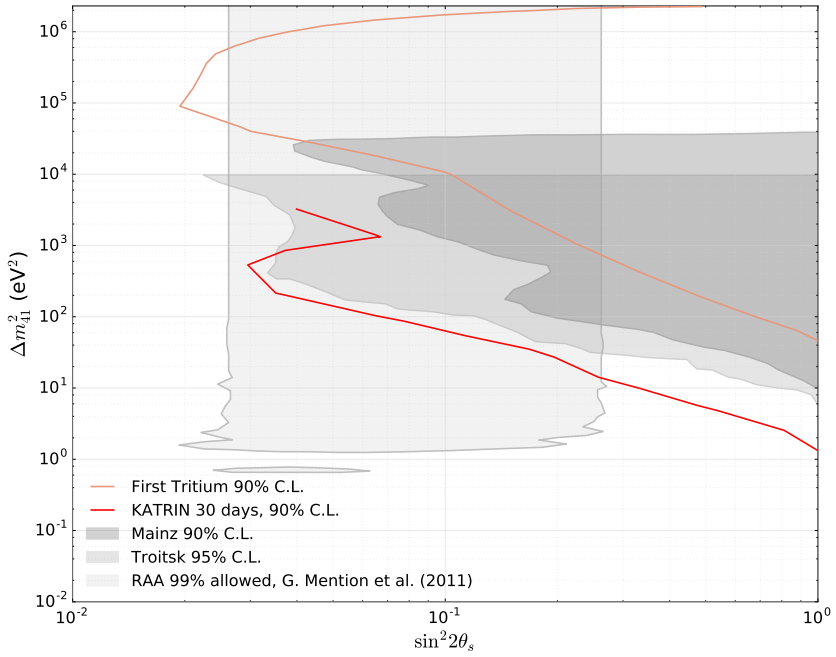

Figure 3.11: The exclusion curve of the analyzed FT data, in comparison with the ones from Mainz [53] and Troitsk [54]. It is remarkable that only with 30 days of measurement at nominal activity, we can cover most of the parameter space excluded by the Mainz and Troitsk experiments.

Chapter 4

Expected Sensitivity of KATRIN for eV Sterile Neutrinos

In this section, we update the existing studies by using our new analysis tools and the current status of KATRIN. First, we show how the statistical sensitivity can improve with the measuring time. Then, we point out the impact of the present background, which is significantly higher than the one predicted in the design report. In addition to the statistical sensitivity, we also study how the projected systematic effects will affect the final results of KATRIN in three years. We end this chapter by providing a comparison of how different scanning ranges and measurement schemes can impact the analysis.

4.1 Statistical Sensitivity

As a first step, we consider the statistical sensitivity of KATRIN for different run times.

Figure 4.1 shows the statistical sensitivity for 30 days, 6 months, and 3 years, with the nominal KATRIN settings. As expected the exclusion gets better with time. Another feature of KATRIN that is made clear here is how fast the sensitivity limits converge. The sensitivity gain from the first 6 months of data is almost the same as the gain from additional 30 months. This means that the statistics needed to resolve the basic spectral shape are acquired relatively fast, and then although KATRIN still improves from statistics, the gain is getting lower.

4.2 Impact of Elevated Background

4.2.1 Impact of Elevated Background

In the KATRIN design report in 2005 [38], the background rate that was expected for the experiment was 10 mcps (milli-counts per second). The now measured

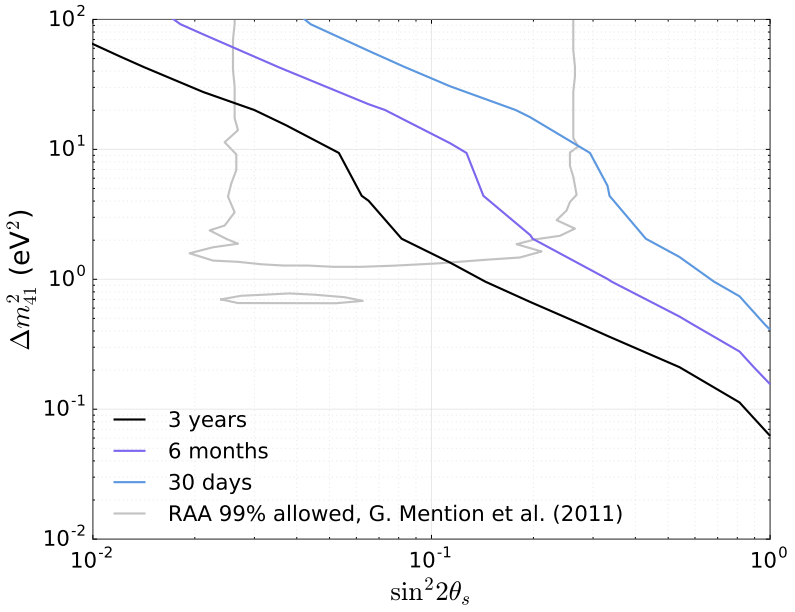

Figure 4.1: Exclusion curves for different measuring times.

background rate of KATRIN is ~685 mcps. This large background rate is attributed mainly to Rydberg atoms coming from the radioactive decay of ^{210}Pb in the walls of the main spectrometer. These atoms have electrons with high principal quantum number, making the electron loosely bound to the atom. Room temperature thermal radiation can free those electrons, which are then accelerated to the same energies as the electrons coming from the source. The different mechanisms concerning Rydberg atoms in KATRIN are discussed in [55].

The higher background can influence negatively the sensitivity of the experiment. Especially for the case of the sterile neutrino, whose signature in the spectrum is expected to be weak, given the preferred small mixing angles, the addition of a background rate can prove a hindrance to our analysis. To visualize the effect of the higher background, we show the impact of the sterile neutrino on a β-decay spectrum, without a neutrino mass, in figure 4.2a. For the plot, we subtract one from the ratio to make the impact strength more clear. The values for the sterile neutrino used for the generation of the spectrum are $m_s = 1$ eV and $\sin^2\theta = 0.1$.

The more pronounced the signal is, the easier the distinction of the two spectra is. The effect of a 10-times larger background, has already a large impact on the sterile neutrino signature, with a threefold reduction of its amplitude.

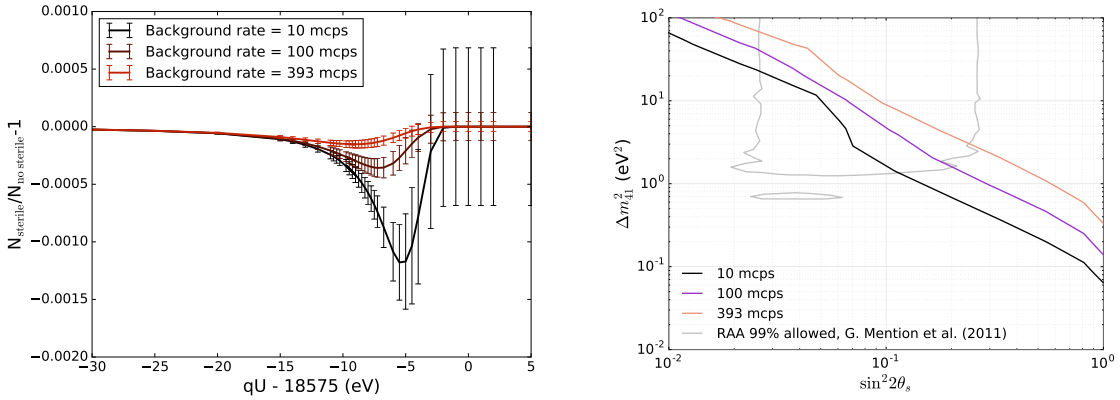

(a) (b)

Figure 4.2: The impact of the higher background in the spectrum (a), has also a clear effect in the sensitivity (b).

To see how this impacts our sensitivity, we consider nominal systematics, 3 years of measurement time and a flat MTD spanning just 30eV below the endpoint. In figure 4.2b we see the exclusion curves for different backgrounds. The higher background makes a great difference even without considering other systematic effects. The curve lies above the best fit of the RAA, situated at $\Delta m_s^2 = 2.3\ \mathrm{eV}^2$ and $\sin^2 2\theta = 0.14$, which means that KATRIN will not be able to completely resolve the anomaly.

The translation and dampening of the signature have to be taken into account for the final sensitivity studies, by spending more time measuring at the retarding potentials close to it. But first, we can explore some means of reducing the background.

4.2.2 Means to Reduce the Background

The background rate can be effectively reduced by increasing the magnetic field in the analyzing plane. We can see from equation 2.5 that if we increase the magnetic field in the analyzing plane, because the magnetic flux stays constant, the area of the analyzing plane has to shrink. The magnetic field of the analyzing plane is thus approximately inversely proportional to the volume of the main spectrometer's flux tube. It turns out that a large portion of the background is proportional to this volume. This behavior, was studied in [55], and is shown in figure 4.3a. In the same plot, the MAC-E filter energy resolution is shown, as it also scales with B_{ana}. The drawback of increasing the magnetic field to reduce the background is that the energy resolution is worsened. We attempt to find the best setting for B_{ana} to be used in the analysis.

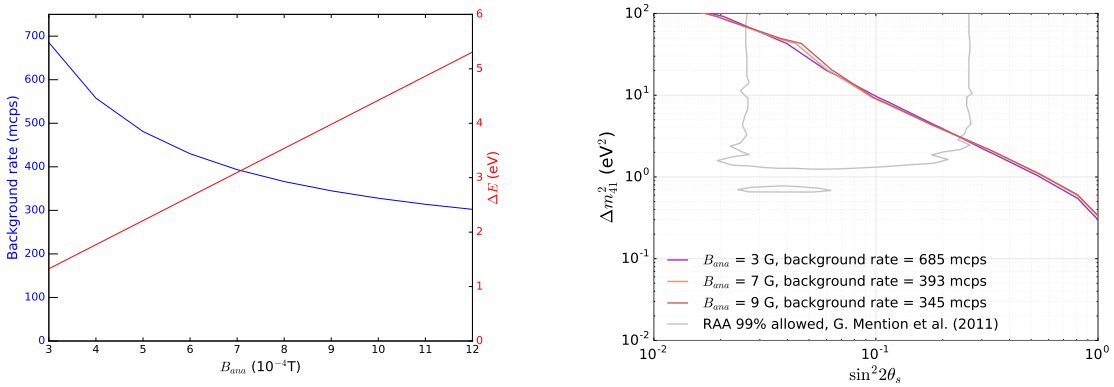

(a) (b)

Figure 4.3: (a) The background rate (*blue*) of KATRIN and the resolution of the MAC-E filter (*red*), plotted against B_{ana}. (b) Three different exclusions for different configurations of B_{ana} and background rate. We see that the variation of the background with respect to the magnetic field of the analyzing plane is not of any importance for the analysis of sterile neutrinos.

We can see that the point where the absolute resolution and background rate are the smallest is for B_{ana} = 7 G. This "optimum" defines the settings at which we achieve the best energy resolution, with the lowest background rate possible (393 mcps). We show how increasing the magnetic field in the analyzing plane to reduce the background affects our sensitivity in 4.3b.

This result shows that for the light sterile neutrino analysis these settings have almost the same impact, thus producing a similar result when tuned simultaneously. While the reduction of the background rate can greatly enhance the sterile neutrino signal, the energy resolution seems to have the exact opposite effect on the sensitivity. We can only improve our sensitivity if the background rate is reduced overall, without changing the magnetic fields. For this reason, we kept the B_{ana} value at 7 G, as this is the value that will most probably be used for the regular KATRIN neutrino mass analysis.

4.3 Impact of Systematic Uncertainties

In this section we discuss the impact of the most important systematic uncertainties. The precise quantification of some of the systematic parameters requires future calibration campaigns or new calculations. For instance, the energy loss func-

Table 4.1: Table listing the values of the different systematics included in the sensitivity studies.

	30 days	3 years best	3 years worst
$\rho d\sigma$	2-3%	0.2%	0.2%
FSD normalization	1%	negl.	1%
FSD shape	P_{GS}(4%),P_{ES}(18%)	negl.	P_{GS}(4%),P_{ES}(18%)
Energy loss fn.[50]	Abdurashitov (D_2)	negl.	Abdurashitov (D_2)
B_s, B_{max}	2.5%, 0.2%	0.2%	0.2%
B_{ana}	1%	0.2%	0.2%

tion has to be precisely recalculated, as the one we use now is an older result of an external group and does not necessarily reflect the exact energy loss function of the KATRIN source. The FSD is also an older result, taking into account that KATRIN will only measure 30 eV below the endpoint. Moreover, as mentioned earlier, the normalization of the excited states and overall variance still suffer from a percent level uncertainty. Accordingly, we consider here a “best-case” and “worst-case” scenario.

Furthermore, we anticipate that our understanding of the systematic may improve over time. The systematics considered here are:

- The column density ρd,
- The FSD,
- The energy loss function,
- The magnetic fields’ strength.

Table 4.1 summarizes the systematics budget used for the best and worst case scenario in three years, as well as for the first 30 days of data taking.

In three years we hope that most of those uncertainties will have been resolved, either by measurements in KATRIN or by other experiments. This is what we signify as "best", which is also the best case scenario at this moment. Of course this scenario is subject to new technologies and analysis methods that can be developed in the following years. As such, these systematics represent our best estimation now, but the knowledge on them might still improve.

The worst case scenario, shown in the third column of 4.1, includes systematics that we do not know if they will be resolved by then, and are mostly associated with independent work outside of KATRIN or special measurements.

We show the impact of the best and worst case systematics in figure 4.4. It seems the addition of the energy loss function and the FSD does not change the sensitivity by much. This is however to be expected, as the electrons have not scattered much in the 30 eV range and moreover the excited states probability in the FSD, which is lesser known, kicks in above 20 eV. First of all, impactful systematics such as the column density and the magnetic fields have the same uncertainty in both cases, as they are the systematics that can be measured and improved from the KATRIN collaboration itself. Furthermore, we scan only 30 eV away from the endpoint of the spectrum, so we are still at the point where the FSD and energy loss are known with great precision and we are dominated by statistics, rather than by systematics.

Still the effect of systematic effects and the higher background can prove detrimental to KATRIN's performance in solving the RAA. The most intuitive way to improve the sensitivity is to aqcuire more information on the shape of the spectrum. This can in general happen by changing the depth of the scan, and the distribution of our measurement points.

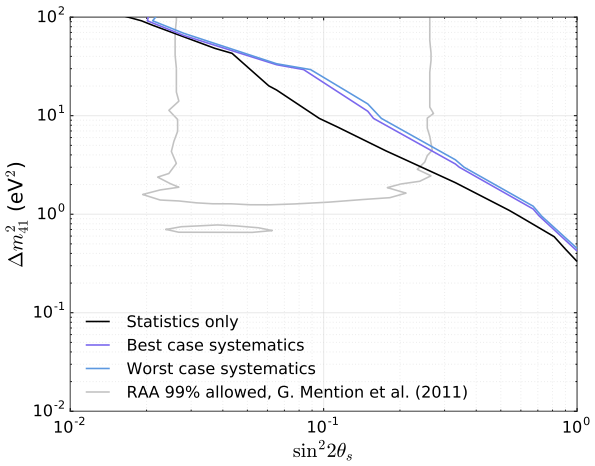

Figure 4.4: KATRIN exclusion for the best and worst predicted systematic uncertainties. By including uncertainties on the FSD and the energy loss function, the exclusion curves do not become much worse.

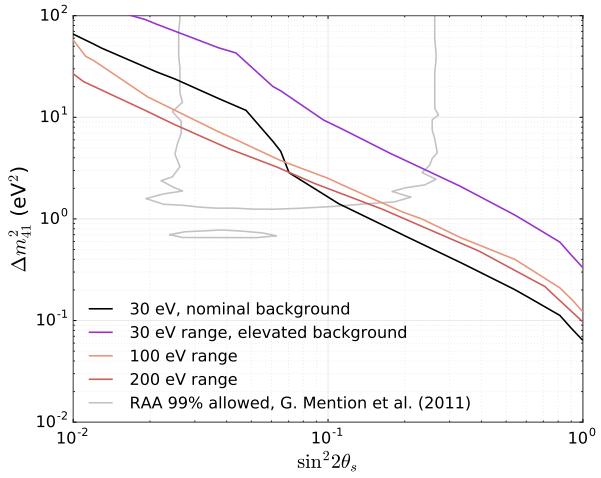

Figure 4.5: KATRIN exclusion for different scanning ranges. By scanning deeper into the spectrum we have more information on the shape of the spectrum, thus being able to better distinguish a sterile neutrino signature.

4.4 Optimization of Measurement Interval

A possibility to compensate for the elevated background rate could be to increase the measurement interval. By measuring deeper into the spectrum we get more information on the shape and by having those additional statistics we can determine the effective endpoint much more precise. The gain in sensitivity is visualized in figure 4.5.

As the detector cannot handle too great rates, we limit our studies to a maximum depth of 200 eV below the endpoint. This is also a range, which is still close to the range for which our model is made. Even though we could fit the FT data that went 1.6 keV below the endpoint well, we cannot be sure that unknown systematics do not appear when we increase the measurement interval by so much. As such, we stick to realistically possible scan ranges, 200 and 100 eV below the endpoint.

Even with the current background, we can almost regain all the lost sensitivity just by increasing the measurement interval. However, the deeper we go into the spectrum, the smaller the impact of the sterile neutrino is, so the gain after the 100 eV range is minimal.

A drawback of this method is that the impact of the systematic uncertainties increases proportional to the measurement interval. Figure 4.6a shows the sensitivity

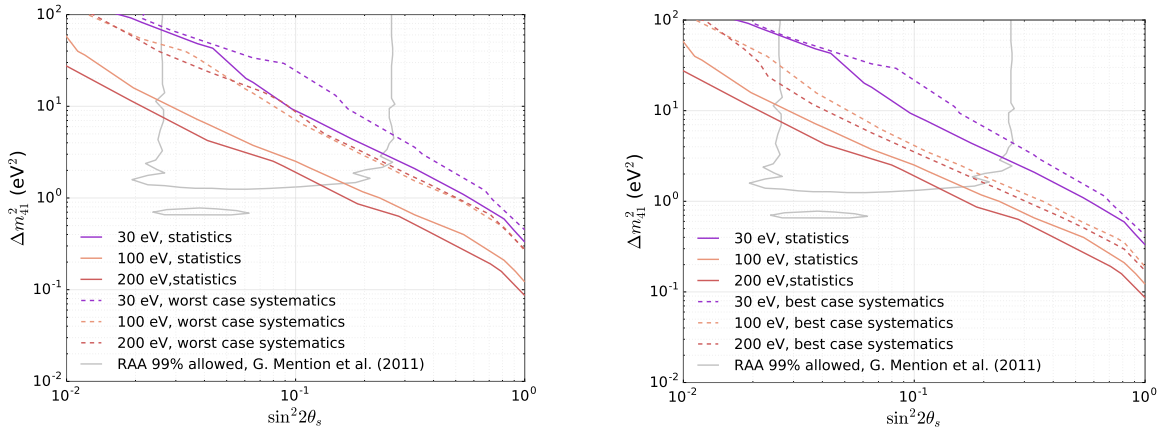

(a) (b)

Figure 4.6: Sensitivity for different scan ranges. We see in (a) that the deeper we scan, the more impact the systematic effects have. However, if the systematic uncertainties are low enough, as is our best case scenario (b), scanning deeper can still improve the sensitivity.

for the different scanning interval, including the worst case systematics. The importance of systematic uncertainties at larger ranges is clear, as the sensitivity for the 200 eV range becomes the same as the one for the 100 eV range.

The difference is due to the uncertainties on the FSD and energy loss function, and this is explained in figure 4.6b, where the best case systematics are included. Here, the hierarchy of the curves is retained, with the 200 eV interval being still better, in contrast to our observation before.

We can already infer that the best range would be the 100 eV, as further increasing the scan range also increases the complexity of the measurement time distribution, except from possibly introducing additional unknown systematics. Even considering the best case systematics, the gain in sensitivity by further increasing the scanning interval is minimal. So we conclude that the best range for KATRIN to search for light sterile neutrinos is to scan to 100 eV below the endpoint.

4.5 Improvements on the Measurement Time Distribution

How much time and at which retarding potential we will measure during one run is called the Measurement Time Distribution (MTD) in KATRIN and plays a significant role in the analysis, as it dictates the most important regions of the spectrum.

For example, it can be tuned so as the measurement can focus on important

regions of the spectrum, such as the spectral distortion in figure 4.2a. Gathering more statistics in the area of the signal can greatly improve our sensitivity, and that is why we showcase four different studies done to derive the MTD for the final analysis.

Out of the four possible MTDs, two were constructed by hand, and two using optimization software from the KATRIN collaboration. We chose a scanning depth of 90-100 eV below the endpoint, according to our short analysis in the previous section. We used the best case systematics, and three years worth of statistics. Figure 4.7 shows the distribution of the measurement points.

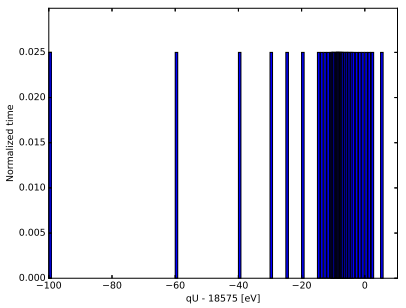

(a) Flat MTD

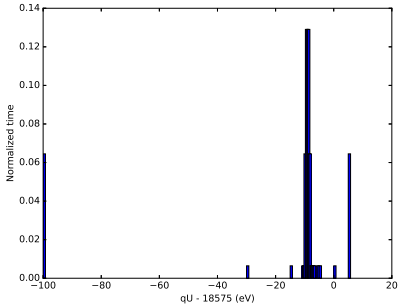

(b) Spiked MTD

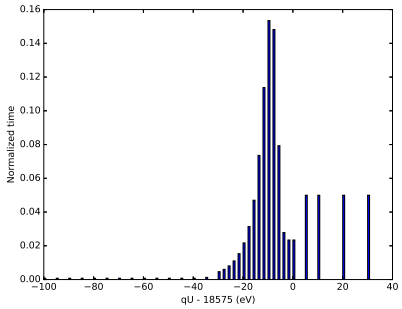

(c) ISOstat MTD

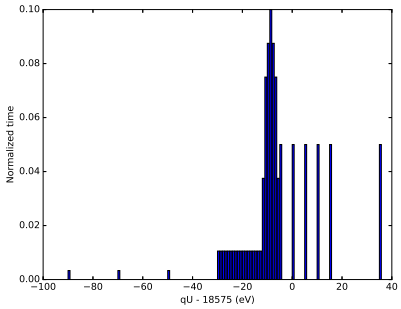

(d) Numerically optimized MTD

Figure 4.7: Four MTDs used for comparison. (a) and (b) were done by hand, whereas (c) and (d) were derived numerically. All of them spend more time on the region where a spectral distortion would be more pronounced. The *spiked* MTD has a lower binning size to visualize a measurement with very few measurement points.

We call the first two MTDs considered, "flat" and "spiked", though their main difference lies in the binning size in the endpoint region. The "ISOstat" MTD is

an MTD that is optimized to yield almost the same statistics in the whole of the spectrum. To achieve that, more time is spent on the points near the endpoint and less time deeper into the spectrum. The last MTD 4.7d is optimized for the first measurements of KATRIN and that is why it contains significantly more points in the background region. As the background is the most important problem we are facing, knowledge on it can help refine the analysis. It is important to note, that the last two MTDs were optimized for the active neutrino mass measurements and not for the sterile one. The signature in the spectrum is in almost the same region for the active neutrino as for the sterile. So we do not expect great deviations, but still draw the exclusions, as the final MTD of KATRIN will most probably look like that.

The comparison of the MTDs is realized with an exclusion plot, shown in 4.8. The importance of the bin size is clear, with the "spiky" MTD delivering worse limits than the "flat" one. Morever, we see that the ISOstat and the optimized MTD return the same results as the manually generated "flat" one. This behavior rests most probably to the fact that the sensitivity can become better by including even two intermediate points between the deepest point and the region of the signal signature, but just adding one measurement point deeper into the spectrum does not help much. Moreover, the three MTDs with higher resolution all spend a notable amount of time in the region of interest, and their difference cannot be made clear in the 3 years of measurement case, where we would anyway have amassed great statistics.

The effect of the different MTDs in less time and without systematics was not considered in this study, but their difference should probably more pronounced than in the case examined here.

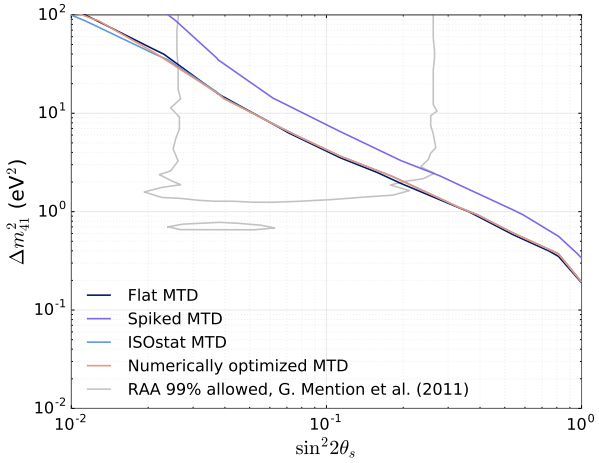

Figure 4.8: Sensitivity from the four MTDs in 4.7. The low resolution, "spiked", MTD shows significantly lower sensitivity. All the other MTDs result in the same exclusion, although being significantly different.

Chapter 5

Conclusion

In this work, a search for light sterile neutrinos with a 3-day data set of the First Tritium measurement campaign was performed. A detailed study of the impact of all relevant systematic effects was performed and revealed that the uncertainty in the determination of the DT concentration was the limiting factor of this measurement. As the amount of the tritium isotopologe in future measurements will be significant higher (100% T_2 as compared to 1% DT) the measurement uncertainty is expected to be drastically reduced.

A very good agreement between the predicted sensitivity to light sterile neutrinos of the First Tritium measurement and the actually achieved exclusion limit could be demonstrated, which shows that the analysis methods and systematic uncertainty treatment is robust.

The 90% C.L. exclusion limit achieved with this data set already tackles the allowed parameter range of the RAA in a high mass range, where dedicated oscillation experiments are not sensitive.

The second focus of this work was the investigation of the KATRIN senstivity to light sterile neutrino, considering an elevated background rate. Here, the effect of the higher background on the sterile neutrino signal was probed and studied. First, the dependence of the background rate on the magnetic field strength in the analyzing plane was checked but it ended up being insignificant for the sterile neutrino. Two different predictions for our knowledge of systematic effects after three years were made and applied to the sensitivity with the elevated background rate.

One solution to regain the past sensitivity is increasing the measurement interval. However, it was shown in figure 4.6 that the deeper we scan, the more pronounced the systematic effects become in the sensitivity. Only by assuming a very optimistic systematics budget (no uncertainty on the FSD and energy loss), the sensitivity can be increased by scanning deeper into the spectrum.

As a result, this work shows that a reduction of the background rate is of upmost importance for the KATRIN experiment to achieve its targeted sensitivity for sterile neutrinos. Several promising methods are being implemented at the moment that have a high potential to reduce the background to its design value of 10 mcps.

Bibliography

[1] Laurie M Brown. »The idea of the neutrino«. In: *Physics Today* 31.9 (1978), p. 23.

[2] Frederick Reines and Clyde L Cowan. »The neutrino«. In: *Neutrinos And Other Matters: Selected Works of Frederick Reines*. World Scientific, 1991, pp. 548–551.

[3] M. Goldhaber, L. Grodzins and A. W. Sunyar. »Helicity of Neutrinos«. In: *Phys. Rev.* 109 (3 1958), pp. 1015–1017. DOI: 10.1103/PhysRev.109.1015. URL: https://link.aps.org/doi/10.1103/PhysRev.109.1015.

[4] S. N. Gninenko, D. S. Gorbunov and M.E. Shaposhnikov. »Search for GeV-scale sterile neutrinos responsible for active neutrino oscillations and baryon asymmetry of the Universe«. In: *Adv. High Energy Phys.* 2012 (2012), p. 718259. DOI: 10.1155/2012/718259. arXiv: 1301.5516 [hep-ph].

[5] Ziro Maki, Masami Nakagawa and Shoichi Sakata. »Remarks on the unified model of elementary particles«. In: *Progress of Theoretical Physics* 28.5 (1962), pp. 870–880.

[6] Juerg Beringer et al. »Review of particle physics«. In: *Physical Review D-Particles, Fields, Gravitation and Cosmology* 86.1 (2012), p. 010001.

[7] Y Ashie et al. »Measurement of atmospheric neutrino oscillation parameters by Super-Kamiokande I«. In: *Physical Review D* 71.11 (2005), p. 112005.

[8] FP An et al. »Observation of electron-antineutrino disappearance at Daya Bay«. In: *Physical Review Letters* 108.17 (2012), p. 171803.

[9] Q Retal Ahmad et al. »Direct evidence for neutrino flavor transformation from neutral-current interactions in the Sudbury Neutrino Observatory«. In: *Physical review letters* 89.1 (2002), p. 011301.

[10] A Aguilar-Arevalo et al. »Evidence for neutrino oscillations from the observation of anti-neutrino (electron) appearance in a anti-neutrino (muon) beam«. In: *Phys. Rev.* 64.hep-ex/0104049 (2001), p. 112007.

[11] Matthew D Schwartz. *Quantum field theory and the standard model*. Cambridge University Press, 2014.

[12] C Patrignani, Particle Data Group et al. »Review of particle physics«. In: *Chinese physics C* 40.10 (2016), p. 100001.

[13] AA Aguilar-Arevalo et al. »Significant excess of electronlike events in the MiniBooNE short-baseline neutrino experiment«. In: *Physical review letters* 121.22 (2018), p. 221801.

[14] KLAUS Eitel, representing the KARMEN collaboration et al. »Latest results of the KARMEN2 experiment«. In: *Nuclear Physics B-Proceedings Supplements* 91.1-3 (2001), pp. 191–197.

[15] P. Adamson et al. »Search for sterile neutrinos in MINOS and MINOS+ using a two-detector fit«. In: (2017). arXiv: 1710.06488 [hep-ex].

[16] R. Acciarri et al. »Long-Baseline Neutrino Facility (LBNF) and Deep Underground Neutrino Experiment (DUNE)«. In: (2015). arXiv: 1512.06148 [physics.ins-det].

[17] Jeffrey M. Berryman et al. »Sterile neutrino at the Deep Underground Neutrino Experiment«. In: *Phys. Rev.* D92.7 (2015), p. 073012. DOI: 10.1103/PhysRevD.92.073012. arXiv: 1507.03986 [hep-ph].

[18] Th. A. Mueller et al. »Improved Predictions of Reactor Antineutrino Spectra«. In: *Phys. Rev.* C83 (2011), p. 054615. DOI: 10.1103/PhysRevC.83.054615. arXiv: 1101.2663 [hep-ex].

[19] G Mention et al. »Reactor antineutrino anomaly«. In: *Physical Review D* 83.7 (2011), p. 073006.

[20] A Gando et al. »CeLAND: search for a 4th light neutrino state with a 3 PBq 144Ce-144Pr electron antineutrino generator in KamLAND«. In: *arXiv preprint arXiv:1312.0896* (2013).

[21] FP An et al. »Search for a light sterile neutrino at Daya Bay«. In: *Physical review letters* 113.14 (2014), p. 141802.

[22] YJ Ko et al. »Sterile neutrino search at the NEOS experiment«. In: *Physical review letters* 118.12 (2017), p. 121802.

[23] I Alekseev et al. »Search for sterile neutrinos at the DANSS experiment«. In: *arXiv preprint arXiv:1804.04046* (2018).

[24] A. P. Serebrov et al. »Sterile Neutrino Search in the Neutrino-4 Experiment at the SM-3 Reactor«. In: *Physics of Particles and Nuclei* 49.4 (2018), pp. 701–708. ISSN: 1531-8559. DOI: 10.1134/S1063779618040482. URL: https://doi.org/10.1134/S1063779618040482.

[25] J Ashenfelter et al. »First search for short-baseline neutrino oscillations at HFIR with PROSPECT«. In: *arXiv preprint arXiv:1806.02784* (2018).

[26] H. Almazan et al. »Sterile Neutrino Constraints from the STEREO Experiment with 66 Days of Reactor-On Data«. In: *Phys. Rev. Lett.* 121 (16 2018), p. 161801. DOI: 10.1103/PhysRevLett.121.161801. URL: https://link.aps.org/doi/10.1103/PhysRevLett.121.161801.

[27] W Hampel et al. »Final results of the 51Cr neutrino source experiments in GALLEX«. In: *Physics Letters B* 420.1-2 (1998), pp. 114–126.

[28] J. N. Abdurashitov et al. »Measurement of the solar neutrino capture rate with gallium metal. III. Results for the 2002–2007 data-taking period«. In: *Phys. Rev. C* 80 (1 2009), p. 015807. DOI: 10.1103/PhysRevC.80.015807. URL: https://link.aps.org/doi/10.1103/PhysRevC.80.015807.

[29] Mario A. Acero, Carlo Giunti and Marco Laveder. »Limits on ν_e and $\overline{\nu}_e$ disappearance from Gallium and reactor experiments«. In: *Phys. Rev. D* 78 (7 2008), p. 073009. DOI: 10.1103/PhysRevD.78.073009. URL: https://link.aps.org/doi/10.1103/PhysRevD.78.073009.

[30] Mona Dentler et al. »Updated global analysis of neutrino oscillations in the presence of eV-scale sterile neutrinos«. In: *Journal of High Energy Physics* 2018.8 (2018), p. 10. ISSN: 1029-8479. DOI: 10.1007/JHEP08(2018)010. URL: https://doi.org/10.1007/JHEP08(2018)010.

[31] R Adhikari et al. »A white paper on keV sterile neutrino dark matter«. In: *Journal of cosmology and astroparticle physics* 2017.01 (2017), p. 025.

[32] Michael Klasen, Martin Pohl and Günter Sigl. »Indirect and direct search for dark matter«. In: *Progress in Particle and Nuclear Physics* 85 (2015), pp. 1–32.

[33] Scott Dodelson and Lawrence M Widrow. »Sterile neutrinos as dark matter«. In: *Physical Review Letters* 72.1 (1994), p. 17.

[34] Peter AR Ade et al. »Planck 2015 results-xiii. cosmological parameters«. In: *Astronomy & Astrophysics* 594 (2016), A13.

[35] Carlos S Frenk and Simon DM White. »Dark matter and cosmic structure«. In: *Annalen der Physik* 524.9-10 (2012), pp. 507–534.

[36] Y. Farzan and A. Yu. Smirnov. »On the effective mass of the electron neutrino in beta decay«. In: *Phys. Lett.* B557 (2003), pp. 224–232. DOI: 10.1016/S0370-2693(03)00207-7. arXiv: hep-ph/0211341 [hep-ph].

[37] S. Mertens et al. »Sensitivity of next-generation tritium beta-decay experiments for keV-scale sterile neutrinos«. In: *Journal of Cosmology and Astroparticle Physics* 2015.02 (2015), pp. 020–020. DOI: 10.1088/1475-7516/2015/02/020. URL: https://doi.org/10.1088%2F1475-7516%2F2015%2F02%2F020.

[38] J Angrik et al. *KATRIN design report 2004*. Tech. rep. 2005.

[39] Christian Karl. »Analysis of First Tritium Data of the KATRIN Experiment«. MA thesis. Technical University of Munich, 2018.

[40] Ch Kraus et al. »Final results from phase II of the Mainz neutrino mass searchin tritium β decay«. In: *The European Physical Journal C-Particles and Fields* 40.4 (2005), pp. 447–468.

[41] V. N. Aseev et al. »Upper limit on the electron antineutrino mass from the Troitsk experiment«. In: *Phys. Rev. D* 84 (11 2011), p. 112003. DOI: 10.1103/PhysRevD.84.112003. URL: https://link.aps.org/doi/10.1103/PhysRevD.84.112003.

[42] Martin Babutzka. »Design and development for the Rearsection of the KATRIN experiment«. PhD thesis. 2014.

[43] S. Lukic et al. »Measurement of the gas-flow reduction factor of the KATRIN DPS2-F differential pumping section«. In: *Vacuum* 86.8 (2012), pp. 1126 –1133. ISSN: 0042-207X. DOI: https://doi.org/10.1016/j.vacuum.2011.10.017. URL: http://www.sciencedirect.com/science/article/pii/S0042207X11003800.

[44] Alexander Jansen. »The cryogenic pumping section of the KATRIN Experiment: Design studies and Experiments for the commissioning«. In: (2015).

[45] J.F. Amsbaugh et al. »Focal-plane detector system for the KATRIN experiment«. In: *Nuclear Instruments and Methods in Physics Research Section A: Accelerators, Spectrometers, Detectors and Associated Equipment* 778 (2015), pp. 40 –60. ISSN: 0168-9002. DOI: https://doi.org/10.1016/j.nima.2014.12.116. URL: http://www.sciencedirect.com/science/article/pii/S0168900215000236.

[46] Lisa Schlüter. »Development of New Methods to Include Systematic Effects in the First Tritium Data Analysis and Sensitivity Studies of the KATRIN Experiment«. MA thesis. Technical University of Munich, 2019.

[47] M Korzeczek. »eV-and keV-sterile neutrino studies with KATRIN«. PhD thesis. Master's thesis, KArlsruhe Institute of Technology, 2016.

[48] VN Aseev et al. »Energy loss of 18 keV electrons in gaseous T and quench condensed D films«. In: *The European Physical Journal D-Atomic, Molecular, Optical and Plasma Physics* 10.1 (2000), pp. 39–52.

[49] Laura Kuckert et al. »Modelling of gas dynamical properties of the KATRIN tritium source and implications for the neutrino mass measurement«. In: *Vacuum* 158 (2018), pp. 195–205.

[50] DN Abdurashitov et al. »Electron scattering on hydrogen and deuterium molecules at 14–25 keV by the "Troitsk nu-mass" experiment«. In: *Physics of Particles and Nuclei Letters* 14.6 (2017), pp. 892–899.

[51] Alejandro Saenz, Svante Jonsell and Piotr Froelich. »Improved molecular final-state distribution of HeT+ for the β-decay process of T 2«. In: *Physical review letters* 84.2 (2000), p. 242.

[52] Magnus Schlösser et al. »Accurate calibration of the laser Raman system for the Karlsruhe Tritium Neutrino Experiment«. In: *Journal of Molecular Structure* 1044 (2013), pp. 61–66.

[53] Christine Kraus et al. »Limit on sterile neutrino contribution from the Mainz Neutrino Mass Experiment«. In: *The European Physical Journal C* 73.2 (2013), p. 2323.

[54] C Giunti et al. »Short-baseline electron neutrino oscillation length after the Troitsk experiment«. In: *Physical Review D* 87.1 (2013), p. 013004.

[55] Nikolaus Rainer-Maria Trost. »Modeling and measurement of Rydberg-State mediated Background at the KATRIN Main Spectrometer«. PhD thesis. Karlsruher Institut für Technologie (KIT), 2019. 178 pp. DOI: 10.5445/IR/1000090450.

Appendix A: Comparison of all studies

We summarize everything in one plot. The combination of the FT data and the three-years KATRIN sensitivity encompass the whole parameter space excluded by the Mainz and Troitsk experiments. Although KATRIN does not seem to reach the best fit values from the reactor experiments, it can exclude more than 80% of the allowed parameter space from RAA.

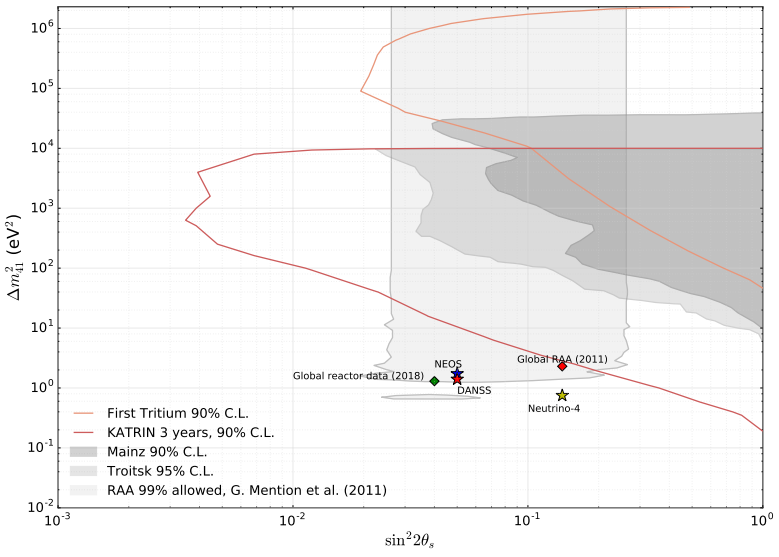

Figure 1: Summary of light sterile exclusions from tritium β-decay, compared to the best fits from reactor experiments [19, 22–24, 30, 53, 54]

Acknowledgements

In the end, I would like to thank everyone in the KATRIN collaboration and TRISTAN group that helped me realize my master's thesis. In particular, I would like to thank Christian Karl and Martin Slezák for their continuous support and outstanding programming skills, without which this analysis would not be possible. I would also like to thank Daniel Siegmann and Tim Brunst for a very welcome and warm atmosphere in our office. Finally, I would like to thank all my friends and family that supported me through this one-year long travel and helped me maintain my mental health despite all the difficulties that arose.